LOCAL MINERALOGICAL VARIATIONS

WITHIN THE LAYERED GABBRO OF

CAPE NEDDICK, MAINE

by

FRANCES M. DAKIN

B.Sc., Bedford College, University of London

(1964)

SUBMITTED IN PARTIAL FULFILLMENT

OF THE REQUIREMENTS FOR THE

DEGREE OF MASTER OF

SCIENCE

at the

MASSACHUSETTS INSTITUTE OF

TECHNOLOGY

September, 1968

Signature of Author_____
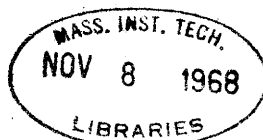
Department of Geology and Geophysics,
September 19, 1968

Certified by_____

Thesis Supervisor

Accepted by_____

Chairman, Departmental Committee
on Graduate Students

LOCAL MINERALOGICAL VARIATIONS WITHIN THE LAYERED GABBRO
OF CAPE NEDDICK, MAINE

by

Frances M. Dakin

Submitted to the Department of Geology and Geophysics
on August 19, 1968
in partial fulfillment of the requirement for the
degree of
Master of Science

Abstract

The Cape Neddick complex provides a compact example
of a layered basic intrusion. An investigation of the
rhythmically layered unit shows that this consists of five
major mineral phases: plagioclase, pyroxene, hornblende,
biotite and magnetite. Modal analyses indicate that the
layers are determined by fluctuations in the relative
proportions of plagioclase, pyroxene and hornblende. The
composition of pyroxene, as determined by X-ray diffrac-
tion analysis, shows slight iron enrichment in dark layers.
The compositions of biotite and hornblende, investigated
by refractive index measurements, show no variation within
the sensitivity of these measurements. A sharp discontinuity
within the layered sequence separates units of very slightly
different mineralogy, one unit containing more serpentine
(primary olivine) than the other.

It is suggested that ionic diffusion played a primary
role in determining the layering, and that the discontinuity
marks the contact of two, chronologically closely spaced,
magmatic phases.

Thesis Supervisor: David R. Wones
Title: Associate Professor of Geology

Table of Contents

Table of Contents Continued

List of Figures

List of Tables

Introduction

Location and previous work

The Cape Neddick complex is an oval stock which intrudes
metasediments of the Kittery formation in southern Maine,
and forms a small promontory to the east of York Beach village.
Its location is shown in Figure 1. The main rock type of the
complex is gabbro, the term 'complex' implying a division
into lithological sub-units, and including many dikes of
varying size, attitude, and composition which cut it.

The earliest detailed description of the gabbro is that
of Wandke (1922b). A brief summary of its lithology is given
as a part of his more extensive work (Wandke, 1922a) on the
intrusive rocks of the Portsmouth Basin. Haff (1939, 1941
and 1943) examined some of the dikes which are included in,
or related to, the complex, and a petrologic description of
the gabbro is presented in his (1939) study of multiple dikes
of Cape Neddick. Gaudette and Sakrison (1959) examined
structural features of the complex, and Gaudette and Chapman
(1964) demonstrated a radial and tangential "spider's web"
pattern in the system of jointing. Eldridge (1960) reviewed
the petrography of the gabbro, and Woodard (1968) has ex-
amined contact reactions between the gabbro and the intruded
metasediments.

The most complete and extensive study is that of Hussey
(1961 and 1962), who has described the petrology, petrography
and lithological construction of the complex, and related it
to two other small basic intrusions in the same locality.

Lithology

Wandke (1922a) distinguished, on the basis of mineralogi-
cal composition, four distinct phases within the complex:
contact phase, gabbro, anorthosite and, forming the center
of the intrusion, cortlandtite. Hussey (1961 and 1962)
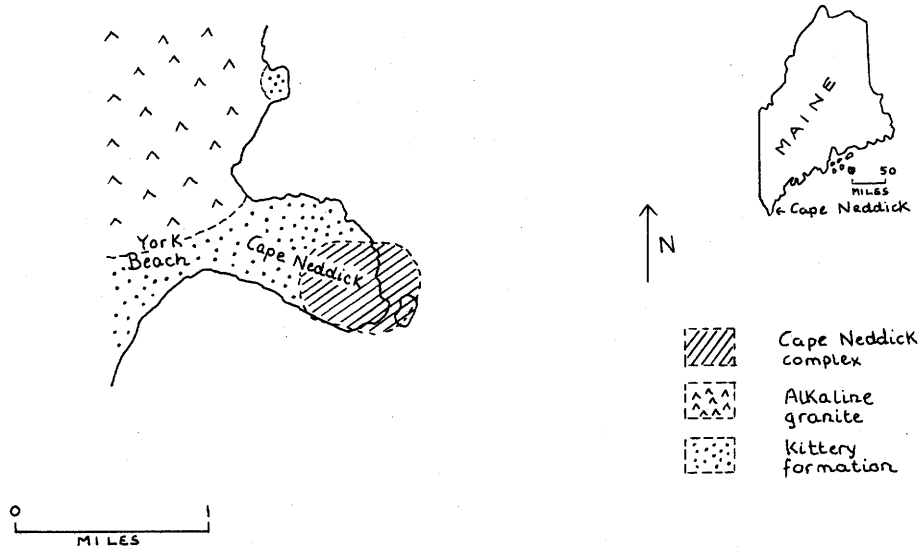
Figure 1. Location of Cape Neddick, and local geological setting (after Hussey, 1962)
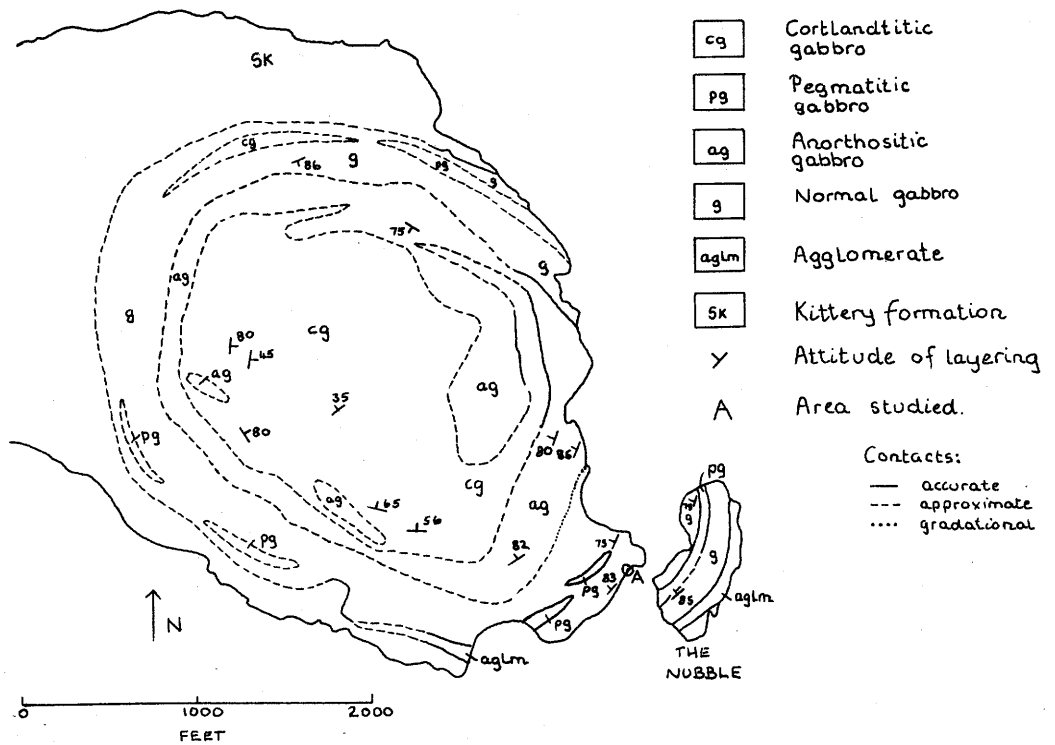
Figure 2. Lithology of the Cape Neddick complex (after Hussey, 1962)

re-examined and modified Wandke's subdivisions, distinguish-
ing five lithological units: agglomerate, gabbroic pegmatite,
normal gabbro, anorthositic gabbro and cortlandtitic gabbro,
as shown in Figure 2. The unit referred to as normal gabbro
is recognized by its medium gray color, and, at a distance
which ranges from 500 to 1,000 feet from the contact, grades
into anorthositic gabbro, which is light gray in color, re-
flecting its largely feldspathic composition. Both these
units show distinct uniform layering, apparently due to regu-
lar fluctuations in the relative proportion of feldspathic
and ferromagnesian minerals, and emphasised by their differential
resistance to weathering, the ferromagnesian-rich layers being
slightly more resistant. The layers form a concentric pattern
around the center of the complex. In the normal gabbro they
lie parallel to the contact with the Kittery formation, dip-
ping steeply inward toward the center of the complex, but
become progressively less steep throughout the anorthositic
gabbro. The center of the complex, and two cresent-shaped
regions within the anorthositic unit, consist of cortlandtitic
gabbro. This unit is rich in ferromagnesian minerals, particu-
larly olivine which is characteristically included in large
poikilitic hornblende crystals. Where exposed, the contact
between the anorthositic and cortlandtitic units is sharply
defined.

Agglomerate is exposed at the eastern and southern con-
tacts of the intrusion. It consists of fragments of the
Kittery formation, and possible near-surface volcanic material.
Gabbroic pegmatite occurrs as lenses within the normal gabbro,
and is characterised by oval-shaped pods of coarse-grained
material.

Hussey (1961) suggests, on the basis of the configuration
and inter-relationships of the three major units (normal gabbro,
anorthositic gabbro and cortlandtitic gabbro), the following
mode of emplacement:

The complex, roughly funnel shaped, was emplaced in two
stages of cone-fracturing as a result of two intrusive phases
of a tholeiitic parent magma. The earlier phase produced the
normal gabbro and anorthositic gabbro, the latter being an

in situ differentiate expressing later crystallization of feldspathic melt. The second phase occurred after a time interval sufficient for at least partial solidification, as indicated by its sharp contact with the first. The same magma was forced upward into the center of the body, and into the two arcuate fractures which are now apparent as cortlandtitic apophyses within the anorthositic unit. The cortlandtitic gabbro represents the early crystalline phases of this second injection, the overlying, feldspathic differentiate having presumably been removed by erosion.

Four types of layering are present in the complex: rhythmic graded layering, rhythmic non-graded layering, sporadic non-graded layering and irregular layering. The distinctive uniform layering of the normal and anorthositic units is of the rhythmic type, both graded and non-graded varieties being present. Sporadic, non-graded layering occurs towards the inner margin of the anorthositic unit, and irregular layering occurs in the cortlandtitic unit.

Statement of the Problem

The origin of small-scale, rhythmic layering in igneous rocks has undergone considerable discussion [see, for instance, Wager (1953, 1959 and 1963), Wager and Brown (1968), Hess (1960), Jackson (1961)] which will be reviewed in a later section. One purpose of the present study is to contribute to this discussion by examining mineralogical and petrographic variations which distinguish alternating rhythmic layers in the Cape Neddick complex. The second purpose is to examine variations associated with a particular type of anomaly in the layering. It was remarked by Hussey, and is clearly shown on observation of the outcrop, that although the layering in the normal gabbro, and the outer part of the anorthositic gabbro, is generally continuous, there are several occurrences of anomalous layering in which one series of layers truncates against another, producing an effect similar to that of cross bedding in sedimentary rocks; or in

which there is a sharp discontinuity between two otherwise
continuous series. The appearance of the first type of
anomaly suggests that it may result from a change in the
direction of flow of liquid from which the crystals are
settling, being in fact an igneous analogy of cross bedding.
The second does not have the appearance of resulting from
a flow mechanism. Two possible explanations are as follows:
firstly, that a block of partially solidified material has
slumped, under gravity, into still molten magma, or secondly,
that a slightly later pulse of magma has intruded, in dike-
like manner, into partially or wholly solidified layered
gabbro. It is proposed, by making close examination of the
layered series on either side of such an anomaly, to detect
mineralogical and petrographic variations which may indicate
its origin.

Procedure

Description of the Area

The area selected for detailed study covers approximately
20 square feet within the unit of normal gabbro, at the eastern-
most tip of Cape Neddick. Its location is indicated by 'A'
in Figure 2, and it is illustrated in detail in Figure 3.
The reason for its selection is twofold. Firstly, it is
located within a region of well developed, non-graded rhyth-
mic layering, and secondly, it demonstrates clearly the type
of anomaly described above. This is shown in Figure 4. The
series of layers on the eastern side of a sharp discontinuity
terminates abruptly, while the series on the western side laps
up against it, curving toward the center of the complex.

As shown in Figure 2, the "topography" of the area falls
into two sections. The landward (upper) section consists of
large, jointed blocks whose interspaces are filled with loose
boulders, and whose vertical walls provide a convenient loca-
tion for core operations. These blocks are in the process
of being worn, altered and broken away by marine erosion.
The seaward (lower) section is low and flat, in effect a
wave-cut terrace which is submerged at high tide. The dis-
continuity described above trends N20°W across the area. It
is easily visible in the flat, seaward section, disappears
beneath a pile of loose boulders in the vicinity of the joint
blocks, and is picked up again on the landward side of these
blocks. On the eastern side of the discontinuity layering
is well developed and distinct, on the western side it is
somewhat less so. On the eastern side of the discontinuity,
and abutting against it, is a roughly rectangular block of
considerably lighter-colored, non-layered material, about 15
square feet in area, whose boundaries make sharp contact
against the darker, layered gabbro. Individual dark layers
of the gabbro are about 1 inch wide; light layers are about
3 inches wide, and the layers dip toward the center of the
complex at an angle of 75° to 80°.

↖ discontinuity
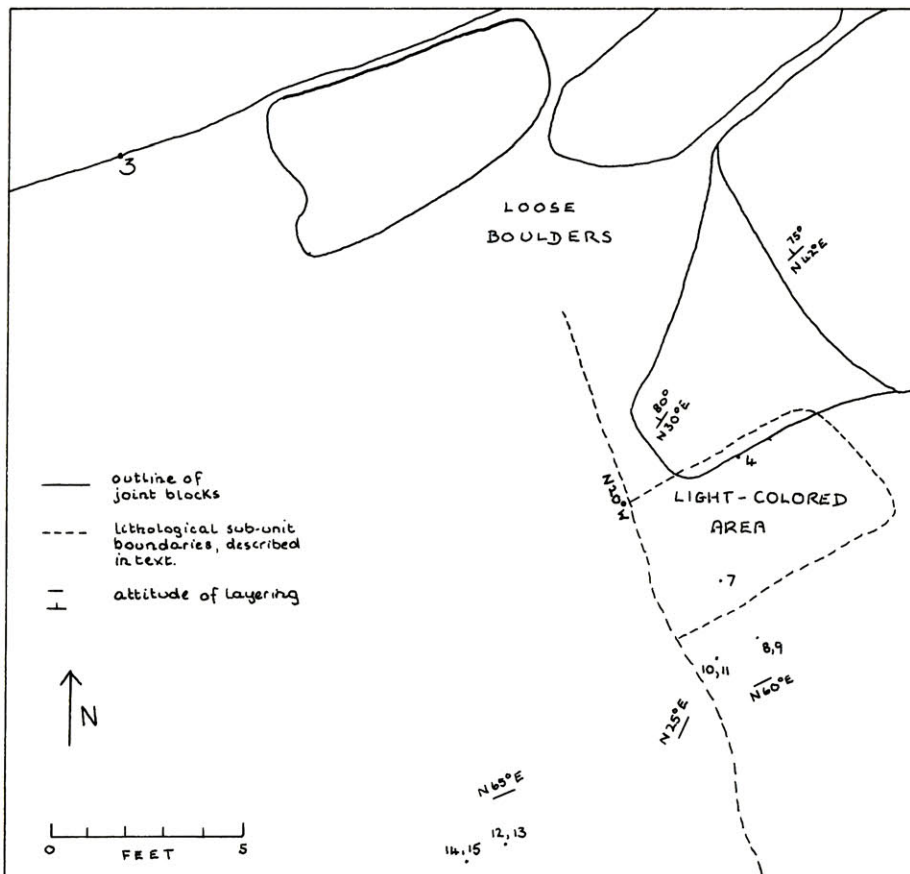
Figure 3. Photograph and sketch map showing the area studied and the locations of samples. The broken line striking N 20° W across the area represents a sharp discontinuity in the layering.

Figure 4. Abrupt discontinuity in the layering of normal gabbro.

Plan of Study

A preliminary survey of the mineralogical composition
of the layered gabbro, including descriptions of the constit-
uent minerals and their textural and paragenetic relation-
ships, is followed by an investigation of four modes of vari-
ation:

(i)   variation in mineralogical composition of light
      and dark layers within a continuous series of
      layers.

(ii) variation in mineralogical composition of the
      layered series on either side of the discontinuity.

(iii) variation in the properties of individual mineral
      phases in light and dark layers within a continuous
      series.

(iv) variation in the properties of individual minerals
      on either side of the discontinuity.

The observations made and results obtained will be as-
similated into a coherent explanation of the process by which
this small area of rock might have formed, in the hope that
extrapolation of the results to more extensive areas might
contribute to the understanding of magmatic processes.

Selection of Samples

Samples selected for detailed examination are numbered
3 through 15, and are located as shown in Figure 3. Samples
3 and 4 are horizontal cores, $1\frac{1}{2}$ inches in diameter, directed
perpendicularly to the layering and of sufficient length to
cut across three or four layers. Samples 7 through 15 are
vertical cores, 0.9 inch in diameter and about 2 inches long.
Sample 7 is taken from the block of light-colored material.
Samples 8 through 15 are taken from the layered regions as
follows: 8 through 11 are taken from the eastern side of
the discontinuity. Eight and 10 are from the same light band
and separated laterally by just over 1 foot; 9 and 11,
similarly separated, are from the adjacent dark band. Samples

12 through 15 have locations analogous to these on the western side of the discontinuity. Twelve and 14 are from the same light band and separated by about 1 foot; 13 and 15 are from the adjacent dark band and have the same separation.

Procedure for Analysis of Samples

Thin sections were prepared from each sample for petrographic study. In core samples 3 and 4 these were cut so as to be oriented both perpendicular and parallel to the layering, thus enabling detection of any preferred orientation of grains. It had been intended to cut the sections from alternate light and dark bands but difficulty arose in that the layering, quite conspicuous upon the outcrop, was hard to detect when the samples were returned to the laboratory. In core sample 3, in fact, it was impossible to detect any evidence of layering, but in 4 it was just possible to distinguish alternate concentrations of light and dark grains. This difficulty in detecting layering in hand samples necessitated the collection of samples 8 through 15, which were carefully selected so as to be from known light and dark layers as seen on the outcrop. Sections from these samples were cut parallel to the layering. The locations and orientations of thin sections from the core samples, together with the location of samples later ground for refractive index measurements and x-ray analysis, are shown in Figure 5. The ground samples were selected so as to correspond as closely as possible to a particular thin section.

Sections from cores 3 and 4 are designated as 3-1, 3-2 etc; and the corresponding ground samples as 3A, 3B etc. Sections and ground samples from cores 7 - 15 are designated by the core number alone.
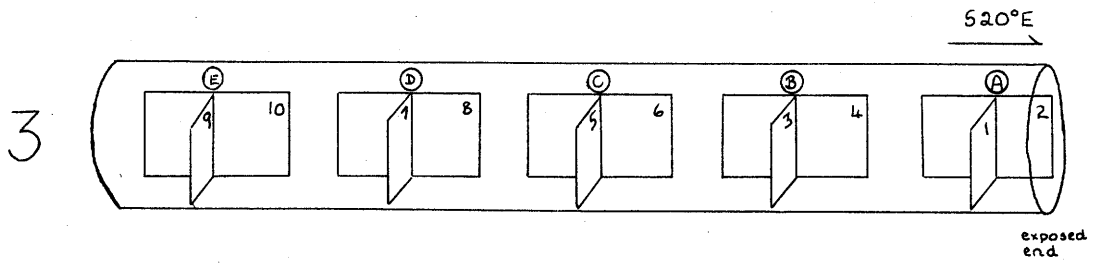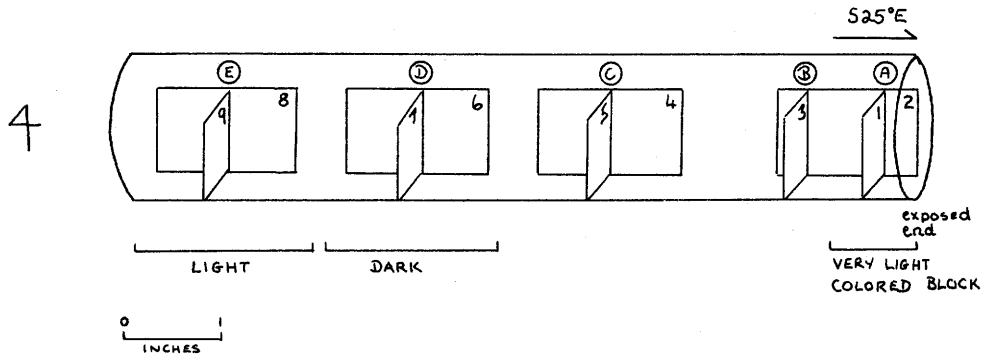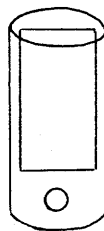
Figure 5. Locations of thin sections (numbered) and ground samples (shown as circles) from core specimens 3 and 4, and 7-15. Dark and light layers are indicated where distinguishable on the core specimen.

Observations

1. Petrology

Observations from a preliminary qualitative study of
the overall composition of the rock, identification and
properties of the constituent mineral phases, and textural
and paragenetic relationships between these phases are
presented below:

A. Mineralogical composition.

The rock consists of five major mineral phases:
plagioclase, pyroxene, amphibole, biotite and magnetite.
Minor constituents, that is, phases which generally form
less than 1% of the whole, are apatite, quartz, alkali
feldspar, ilmenite, carbonate, chlorite, serpentine, sericite
and a trace of zircon.

B. Description of minerals present.

(i) Plagioclase. This occurs as elongate grains,
the subhedral tendency of which is, however, marred by gross
irregularities. Frequently one grain appears to deeply pene-
trate, or be entirely enclosed by, another, and the result
is generally a haphazard intergrowth of grains as shown in
Figure 6. Very occasionally, an extremely irregular, inter-
locking accumulation of tiny, anhedral feldspar crystals, with
a few ferromagnesian grains, occurs, as shown in Figure 7.
Albite twinning is ubiquitous; pericline and Carlsbad twin-
ning are common. There is, however, a rather surprising
scarcity of cleavage. The grains are strongly zoned, the
pattern of zoning shown depending upon the orientation of
a particular grain. One pattern recurs so frequently that
it might be described as typical. It is best shown by grains
whose sections are oriented parallel or sub-parallel to the
{010} planes, and is illustrated in Figure 8. A calcic core
is surrounded by a region of fine, sharply divided oscillatory
zones, and a normally zoned, that is, progressively more sodic,
rim. The zoning may conveniently be studied using a flat-
stage microscope, by selecting sections oriented precisely
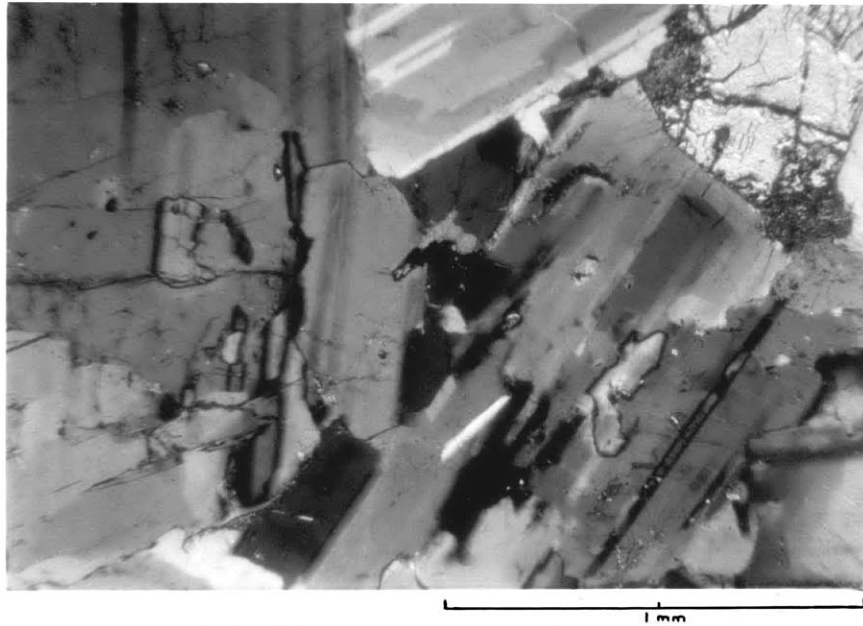
Figure 6. Typical texture in plagioclase. Subhedral outlines are notched and broken, giving an irregularly interlocking matrix. Section 4-7. Cross nicols. x 58.
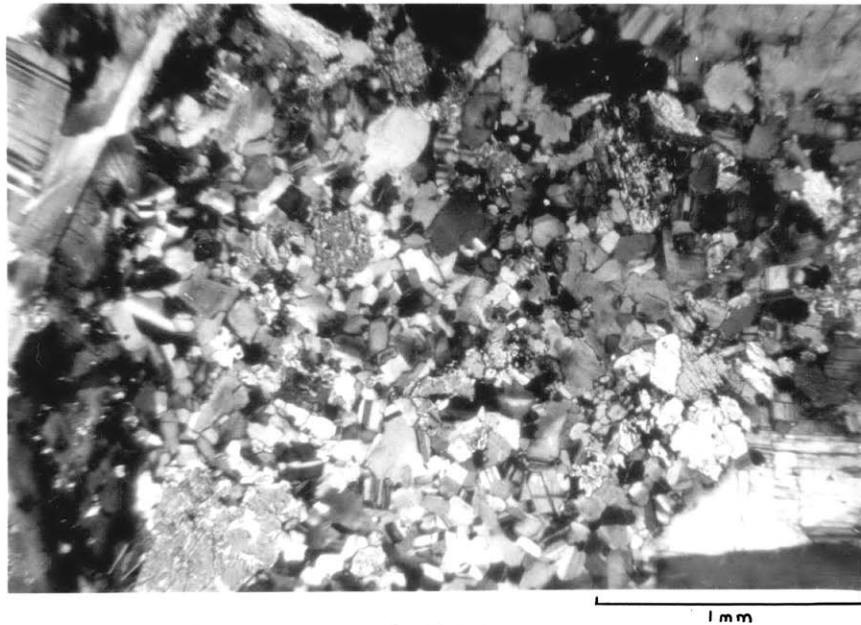
Figure 7. Extremely irregular mass of tiny feldspar fragments, with some pyroxene, magnetite and opaques. Section 3-5. Cross nicols. x 36.
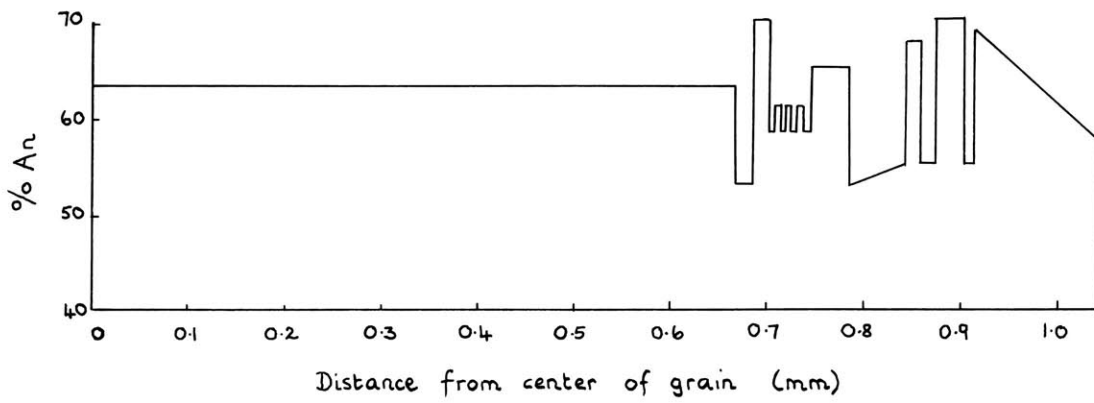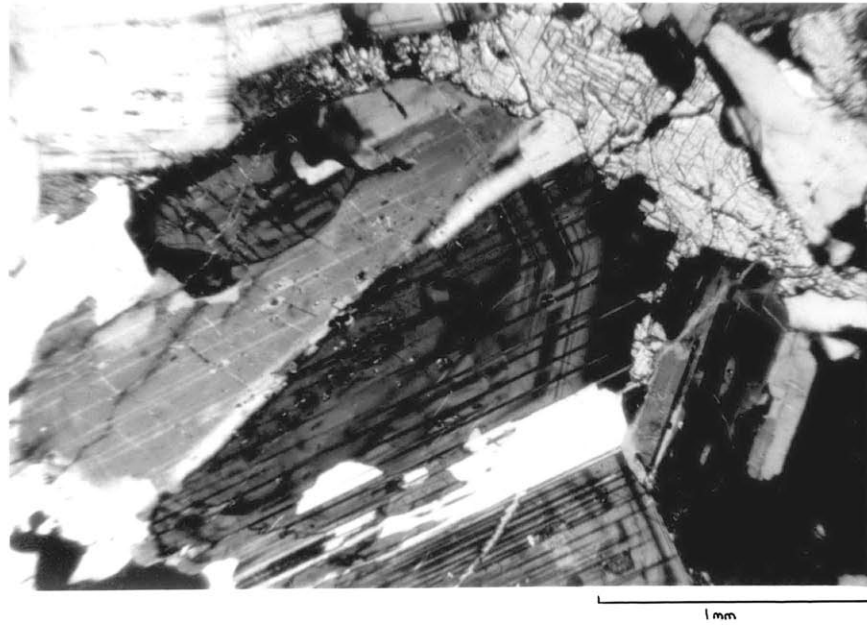
Figure 8. Characteristic zoning pattern in plagioclase. Section 3-1.
Cross nicols. x36. The location of the plotted profile is shown by the
broken line in the photograph.

perpendicular to the Z vibration direction, and measuring the
angle between Y and {010}, the plane of albite twinning. The
plagioclase composition may then be determined from the ap-
propriate curve of Duparc and Reinhard (1924, p. 32). The
core generally shows some patchy zoning, and contains many
small, randomly oriented inclusions of biotite, opaque material,
hornblende and occasional zircon. Within the region of os-
cillatory zoning, zones more calcic than the core itself may
occur. Frequently individual zones are themselves composed
of a series of exceedingly fine oscillations. A few inclusions
may occur within this region. The rim shows a steady decrease
in calcium content toward the edge of the crystal, extending
to what must often be a highly sodic periphery, and is generally
free of inclusions. It is not possible to obtain the precise
composition of the rim by the method outlined above for zoned
crystals, since the optical vibration directions vary with
composition, and a section which is appropriately oriented
for the core will not be so for the rim. The composition
of plagioclase cores shows great variety, averaging about
An_{60} but ranging from An_{50} to An_{70} even in one section.

Measurements by C. M. Spooner (personal communication)
on plagioclases from the normal gabbro, using a 4-axis uni-
versal stage, have shown that an optic angle of 90° cor-
responds to a composition An_{75}. This indicates that the
plagioclase is in a low-temperature structural state.
(Deer, Howie and Zussman, 1963, p. 134).

(ii) Pyroxene. Pyroxene occurs in anhedral grains
which are almost colorless under plain light, with a slightly
pink tinge, and in some sections a hint of pleochroism. It
is optically positive with a moderate optic angle (about 50°)
indicating augite. Maximum interference color is 2° green.
Most sections show characteristic pyroxene cleavage. Twin-
ning, with composition plane {100}, is quite common. In
addition to cleavage, the grains contain many irregular
fractures which are filled with green or brownish green material,
probably chlorite. Most of the pyroxene grains contain tiny,
oriented needle-like inclusions (Figure 9). These inclusions

1μ
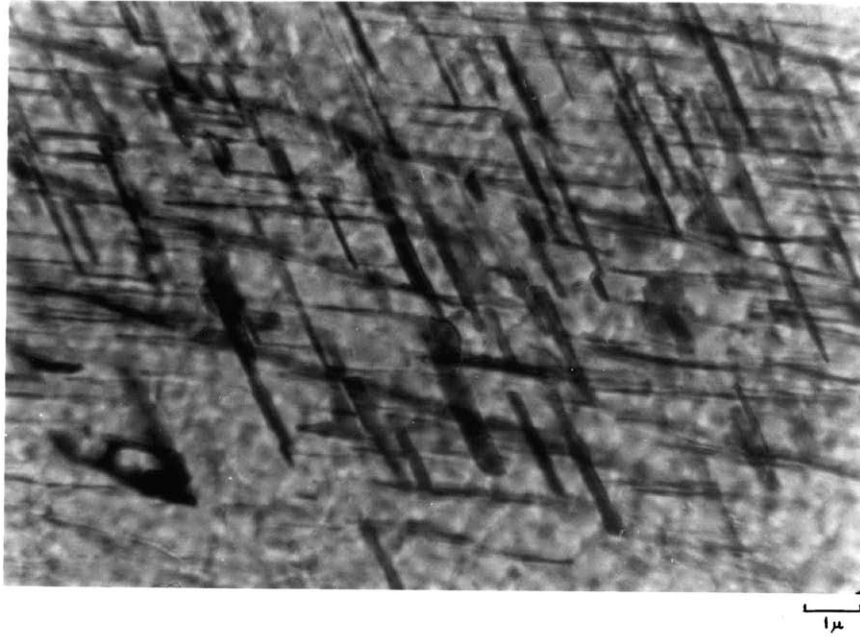
Figure 9.   Oriented inclusions in pyroxene. The continuous dark lines running diagonally across the photograph are {110} cleavage traces. Section 4-7. Ordinary light. × 860.

form clusters, often densely packed and sometimes covering
the entire area of the enclosing pyroxene grain. They are
oriented in two directions, range in length from .005mm -
.05mm and,although dark in color, are not quite opaque. Their
small size makes measurement of their optical properties un-
feasible. Rutile was suspected, on the basis of their general
appearance, and their apparent similarity to a description
of exsolved rutile in orthopyroxene by Moore (1968). Elec-
tron microprobe analysis was used in an attempt to identify
them. Although the inclusions were too small even to permit
focussing of the electron beam upon one individual, it was
hoped to obtain an indication of their composition, particu-
larly their titanium content, by comparing an analysis of a
grain abundant in inclusions with one free from them. The
pyroxene grains analysed were taken from core no. 1, a sample
that was obtained for a preliminary investigation of the layer-
ing and which is not discussed in the present study. It is
located about 15 feet to the east of the northeast corner of
the area shown in Figure 3. The results of the analyses are
presented in Table 1, which compares three small grains, all
free of inclusions, with a grain almost filled by a dense
cluster of them. The results are somewhat inconclusive. The
inclusion-rich grain showed higher titanium than two of the
inclusion-free grains; the third inclusion-free grain, how-
ever, showed just as high a titanium content. Moore (per-
sonal communication) suggested that the inclusions are not
rutile, and a visual comparison of them with the rutile
needles which Moore described also showed obvious dissimi-
larity.

The composition of the pyroxene in terms of atomic per-
centages of calcium, iron and magnesium end members was ob-
tained from the microprobe analysis as $Ca_{43.9} Mg_{43.5} Fe_{12.6}$,
confirming its identification as augite. This composition is
plotted on Figure 21 (in a later section), in comparison
with compositions obtained from x-ray diffraction measurements,
and those of pyroxenes from the layered series of the
Skaergaard Intrusion, East Greenland.

Table 1

Electron microprobe analysis of four pyroxene grains

% weight of oxides

	1	2	3	4
	Pyroxene with needles	Pyroxene free from needles		
FeO	8.3	8.5	8.9	8.3
TiO_2	1.8	1.2	1.8	1.4
Al_2O_3	4.9	3.8	4.9	4.2
MgO	13.6	13.4	13.0	13.3
CaO	21.6	21.4	21.8	21.8
SiO_2	49.9	50.2	51.8	50.7
Na_2O	0.2	0.2	0.2	0.2
Total	100.3	98.7	102.4	99.9

(iii) <u>Amphibole</u>. Amphibole occurs in large, anhedral masses, as flakes within pyroxene grains and as small inclusions in plagioclase cores. It is deep brown in color and shows strong pleochroism as follows:

X	Y	Z
light yellow	yellowish brown	deep brown

The grains are optically negative with a large optic angle (about 80°). The color and pleochroism and large optic angle indicate common hornblende. Maximum interference color is 2° green. Appropriately oriented grains show the characteristic amphibole cleavage and all grains show irregular fracturing.

(iv) <u>Biotite</u>. Biotite occurs as euhedral to subhedral grains, as flakes within pyroxene grains and as tiny inclusions in plagioclase cores. It is deep reddish brown in color, suggestive of high titanium content (Hall, 1941a), and shows the following pleochroism:

X	Y	Z
light yellow	deep red-brown	deep red-brown

The optic angle is very small (2°-3°), and maximum interference color is 2° green.

(v) <u>Magnetite</u>. Magnetite occurs for the most part as large, amoeba-like blobs, and only occasionally as euhedral grains.

(vi) <u>Minor constituents</u>. Apatite occurs as elongated, anhedral grains and, less frequently, as subhedral crystals. The anhedral grains average about 1mm in length, but occasionally are 2mm or longer.

Quartz occurs as subhedral or anhedral grains, readily distinguished from plagioclase by its lack of twinning, inclusions or zoning, and its uniaxial negative interference figure.

Alkali feldspar occurs as anhedral grains, distinguished from plagioclase by its lack of twinning and slightly lower relief. Its large optic angle (70°-80°), slightly cloudy appearance, and response to sodium cobaltinitrate stain indicate orthoclase.

Ilmenite occurs as small, rounded grains, distinguished from magnetite by a yellowish luster in reflected light, in contrast to the blue-gray luster shown by magnetite. Sufficient was collected from sample 4C to prepare an x-ray powder sample and thus confirm its identification. The data used in identification are presented in Table 2.

Carbonate, chlorite, serpentine and sericite are alteration products, and described in the next section.

C. <u>Textural and paragenetic relationships</u>.

The texture is broadly described as hypidiomorphic granular. The most obvious feature is that pyroxene, hornblende and, in general, biotite, are interstitial in a matrix of randomly oriented plagioclase grains. The ferromagnesian minerals appear to have flowed between and around the plagioclase grains, sometimes completely enclosing them, as shown in Figure 10. Their forms are thus completely controlled by the plagioclase interstices. They are not evenly dispersed in the plagioclase matrix, but tend to group into clusters. A comparison of the sections oriented parallel to, and perpendicular to, the layering, reveals no obvious evidence for preferred orientation of any grains.

Relationships between the ferromagnesian minerals themselves are complex, but a general pattern which frequently tends to be followed is illustrated by Figure 10. A pyroxene grain is partially or wholly surrounded by hornblende, which extends away from the pyroxene grain as narrow stringers through feldspar interstices. These stringers terminate in biotite as opaque grains. It must be emphasized that such a pattern is merely a tendency; nevertheless the tendency is considered sufficient to be regarded as significant.

As mentioned above, biotite has a second mode of occurrence: as tiny, subhedral and anhedral inclusions in the central regions of plagioclase grains. Although in such occurrences there is a general tendency for the biotite grains to be aligned in the direction of the traces of the albite twin lamellae, this is by no means the rule, and all orientations are observed. Both biotite and hornblende occur fre-

Table 2. X-ray identification of ilmenite in sample 4C.*

X-ray data for black, non-magnetic material from sample 4C.		X-ray data for ilmenite ($FeTiO_3$) (Posnjak and Barth, 1934)	
**2θ (observed) degrees	d (observed) Å	d Å	hkl
23.812	3.733	3.70	110
32.564	2.747	2.74	121
35.274	2.542	2.53	$\bar{1}10$
40.340	2.234	2.23	120
48.762	1.866	1.865	220
53.087	1.724	1.720	231
61.604	1.504	1.504	130
63.299	1.468	1.465	$\bar{2}11$
Computed cell dimensions		Cell dimensions of ilmenite	
a = 5.531±0.002 Å		a = 5.52	
α = 54°43.3'±0.9'		α = 54°40'	
V = 104.96±0.05 Å		V = 104.6 Å^3	

This data corresponds most closely to the composition $FeTiO_3$
(see Posnjak and Barth (1934) p. 273, fig. 1)
*Refined in rhombohedral system, using computer program written
by Evans, Appelman and Handwerker (1963) and described in a
later section.
** Explanation of symbols

2θ diffraction angle   d interplanar spacing
a cell edge α axial angle
V cell volume
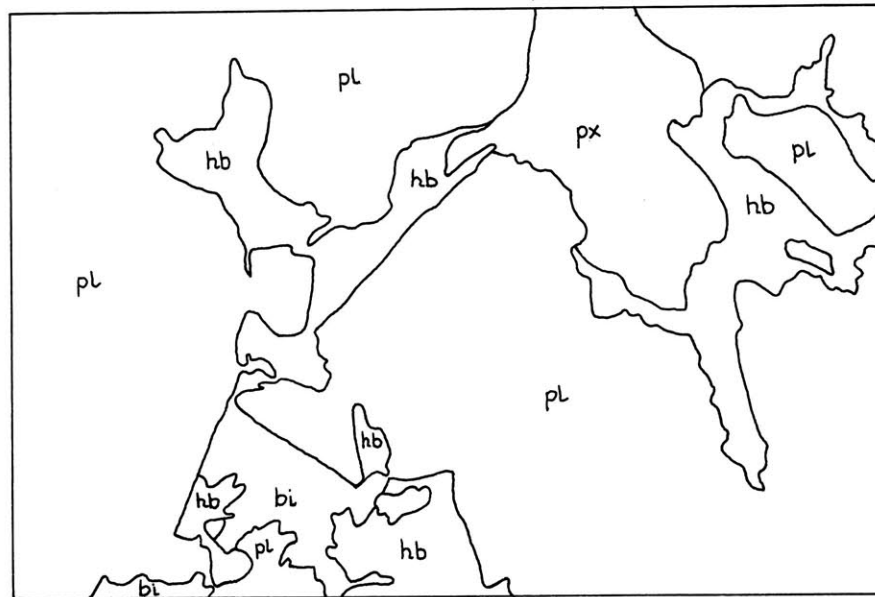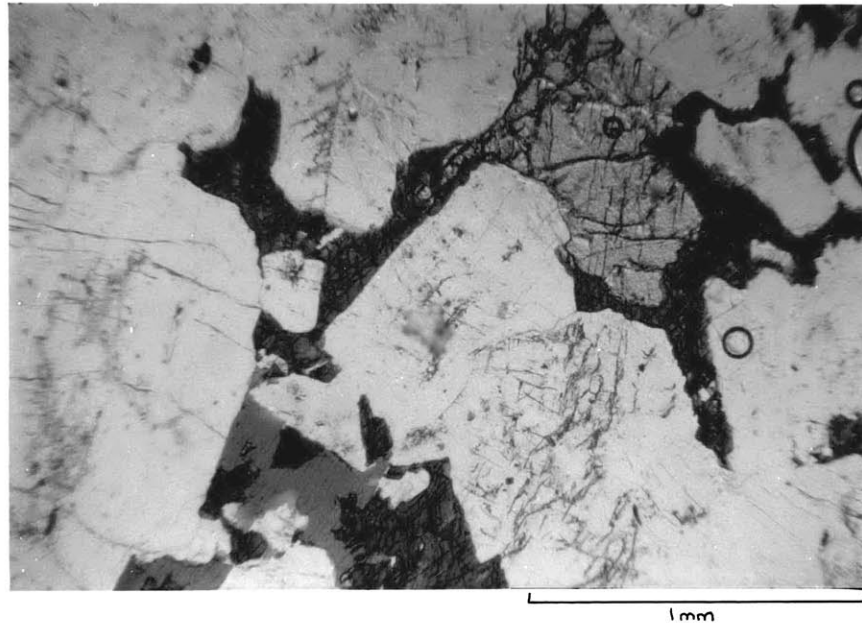
Figure 10. Characteristic occurence and association of pyroxene, hornblende and biotite. The ferromagnesian minerals are interstitial in a matrix of randomly oriented plagioclase grains. Ordinary light. × 45. Section 4-5.

(pl = plagioclase; px = pyroxene; hb = hornblende; bi = biotite)

quently as flakes within pyroxene grains. In some instances,
biotite is enclosed within a hornblende grain, but no occur-
rences of biotite enclosing hornblende are observed.

Magnetite has every possible mode of occurrence. It
occurs as irregular, amorphous masses, as interstitial grains
in the plagioclase matrix, as anhedral or subhedral grains
within all of the major mineral phases, and as small inclu-
sions in plagioclase cores. A particularly characteristic
occurrence is as an intergrowth with biotite.

Ilmenite generally occurs in small, rounded forms within,
or at the periphery of, magnetite grains, but is occasionally
observed within pyroxene.

Apatite may occur within any mineral phase, but is most
frequently observed in the plagioclase matrix. It does not
appear to be confined to the interstices as are the ferro-
magnesian minerals, and the grains are usually rounded and
irregular. Quartz, however, appears to be a part of the
matrix itself, interlocking with the feldspar grains. It
also occurs in association with orthoclase, in a graphic
intergrowth as shown in Figure 11. Both quartz and ortho-
clase are far more abundant in section 7, from the light-
colored block, than in any other section.

Carbonate has several modes of occurence. It may occur
as continuous grains, either independently or together with
chlorite, in plagioclase interstices; as tiny, irregularly
distributed, flaky grains closely associated with pyroxene
and green chlorite; or as regular, oval masses of flaky grains,
generally within pyroxene (see Figure 12). These oval masses
are often associated with serpentine, as described below.
From its association and occurrence, the composition is as-
sumed to be dolomitic.

Chlorite is most conspicuously present as fibrous,
green, fan-shaped aggregates of penninite, characterised by
its anomalous blue interference color. Such aggregates fre-
quently occur in plagioclase interstices, often together with
carbonate. Patches of pale green or greenish brown chlorite
are associated with pyroxene, biotite and hornblende.

Figure 11. Graphic intergrowth of quartz (light) and orthoclase (dark). Section 7-1. Cross nicols. x 176.

Serpentine occurs as fibrous aggregates which have a distinctive pseudomorphic form. These aggregates range from 0.2mm to 3mm in length, and are frequently oval in shape and associated with clusters of ferromagnesian minerals (Figure 12). In no cases, however, do they enclose a ferromagnesian grain. They also occur in interstices in the plagioclase matrix. The serpentine is green to greenish brown in color, and so finely fibrous that its fibrous nature is apparent only under high magnification, and under crossed nicols. The whole aggregate is crossed by irregular fractures. Interference colors range from greenish yellow to reddish brown, having probably been modified by the natural color of the mineral. Due to the fibrous nature of the material it is impossible to obtain an interference figure, and identification as serpentine is on the basis of color, fibrous structure, and pseudomorphic form. Frequently these forms consist of a combination of both serpentine and flakey carbonate, sometimes containing a few grains of magnetite.

A very small amount of sericite is present, as an alteration product of plagioclase.

The following observations are made as to alteration relationships between individual mineral phases:

(i)	Pyroxene altering to hornblende (see Figure 10)
(ii)	Pyroxene altering to hornblende and biotite (Figure 13)
(iii)	Pyroxene altering to carbonate and chlorite (Figure 14)
(iv)	Pyroxene altering to carbonate, hornblende and chlorite (Figure 15)
(v)	Hornblende altering to biotite (Figure 15)
(vi)	Hornblende altering to carbonate and chlorite
(vii)	Biotite altering to carbonate and chlorite
(viii)	Biotite altering to magnetite (Figure 16)
(ix)	Plagioclase altering to sericite.

The significance of these observations will be discussed in a later section.
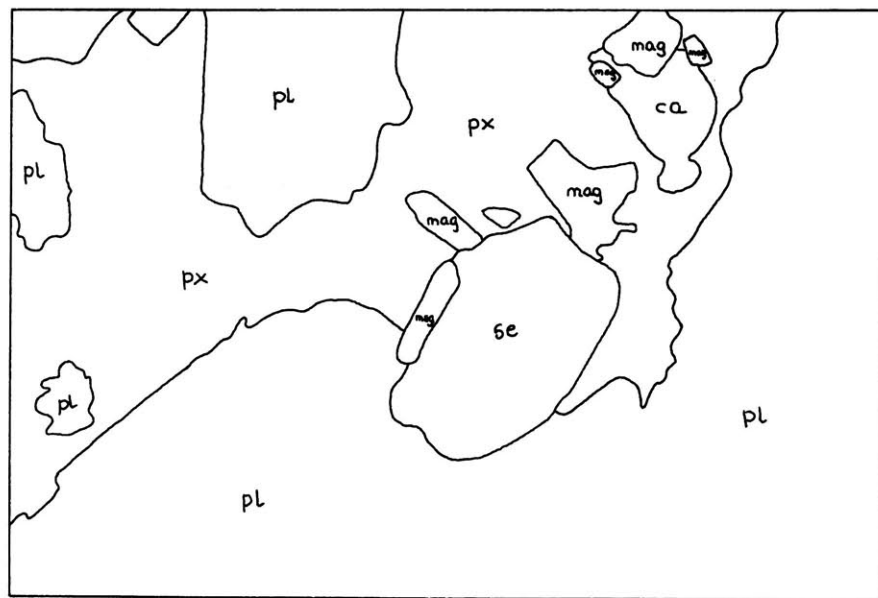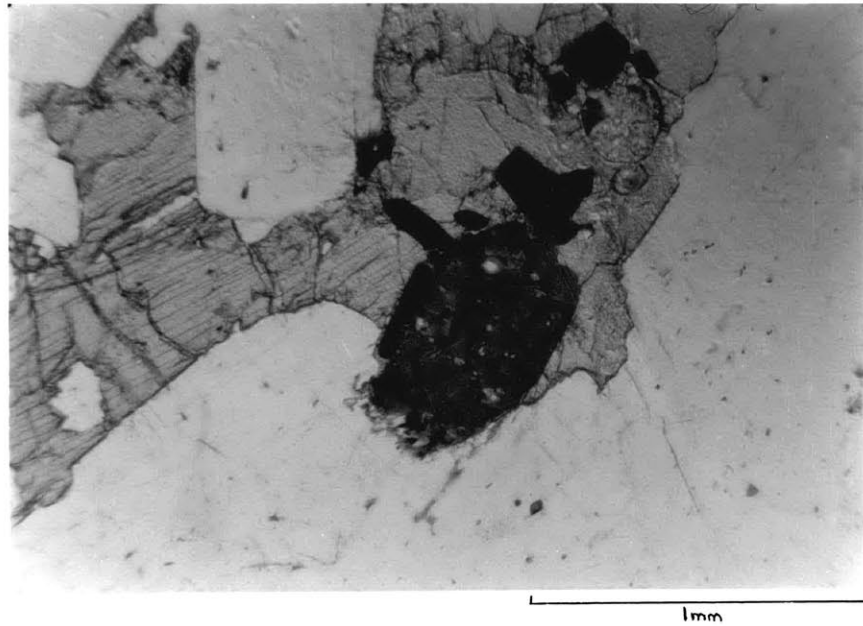
Figure 12 . Serpentine and carbonate aggregates in pyroxene.
These appear to be pseudomorphic forms. Section 3-1.
Ordinary light. x 45
(pl = plagioclase; px = pyroxene; mag = magnetite; ca = carbonate;
se = serpentine)
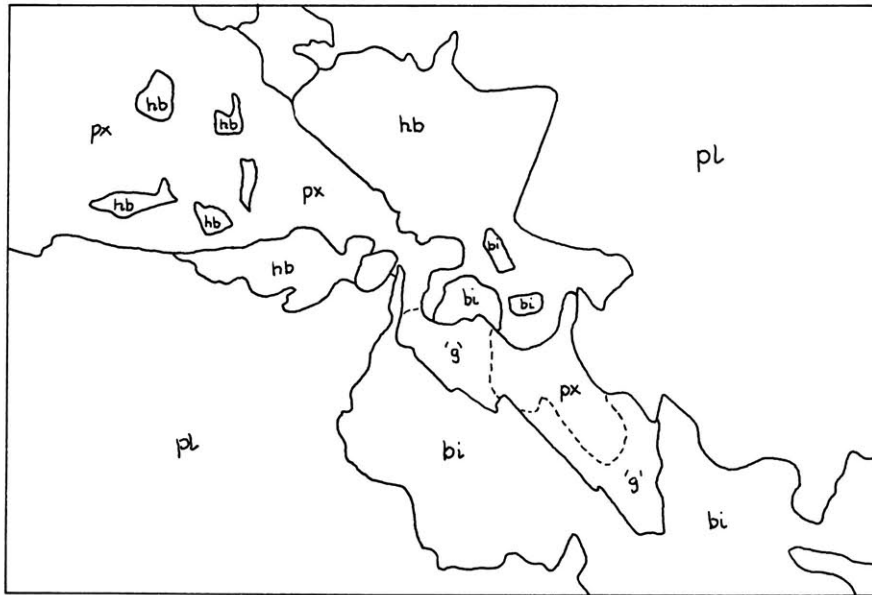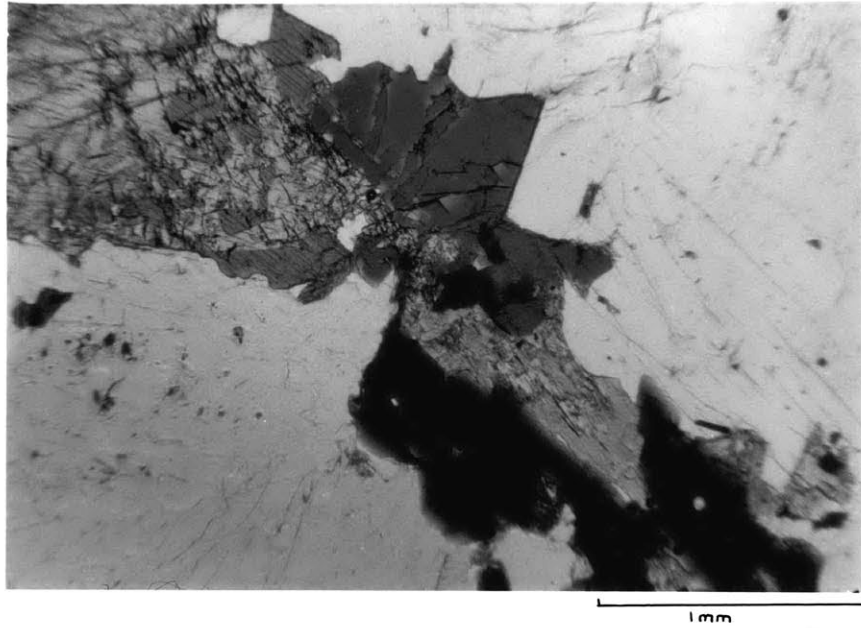
Figure 13. Pyroxene altering to hornblende and biotite. The area of the pyroxene grain marked 'g' represents light green material (possibly chlorite) which appears to be an intermediate stage in the alteration process. Section 13. Ordinary light. x 36. (pl = plagioclase; px = pyroxene; hb = hornblende; bi = biotite)
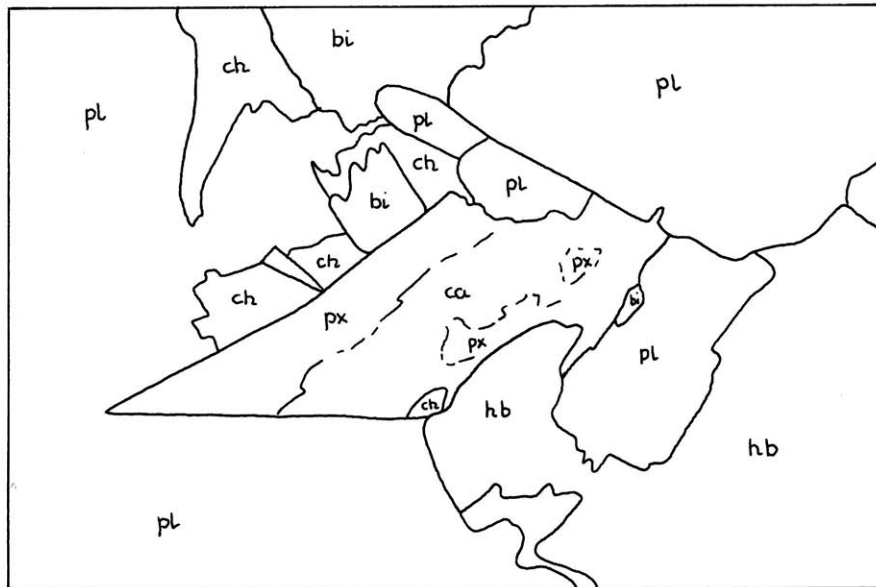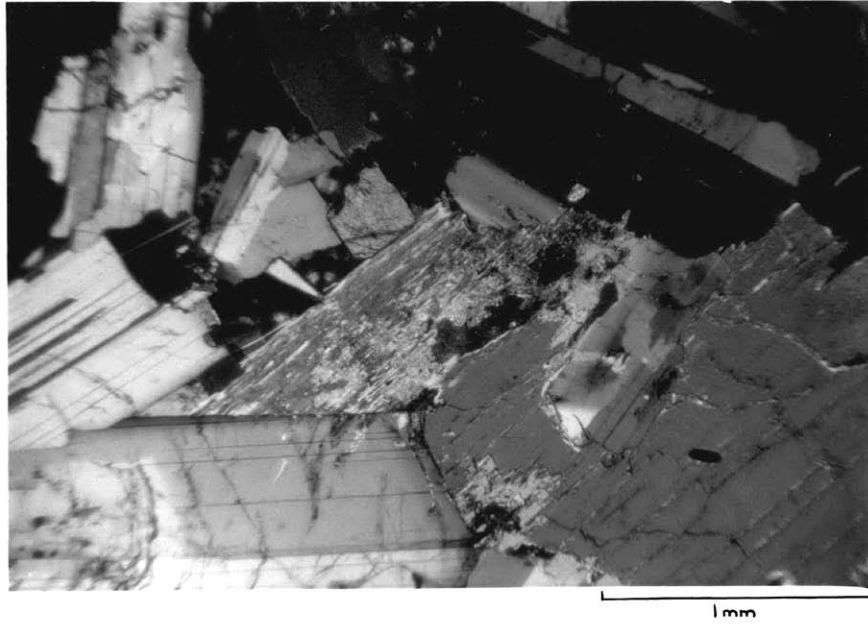
Figure 14. Pyroxene altering to carbonate and chlorite (penninite) Section 4-3. Cross nicols. × 36.

(pl = plagioclase ; px = pyroxene ; hb = hornblende ; bi = biotite; ca = carbonate ; ch = chlorite)
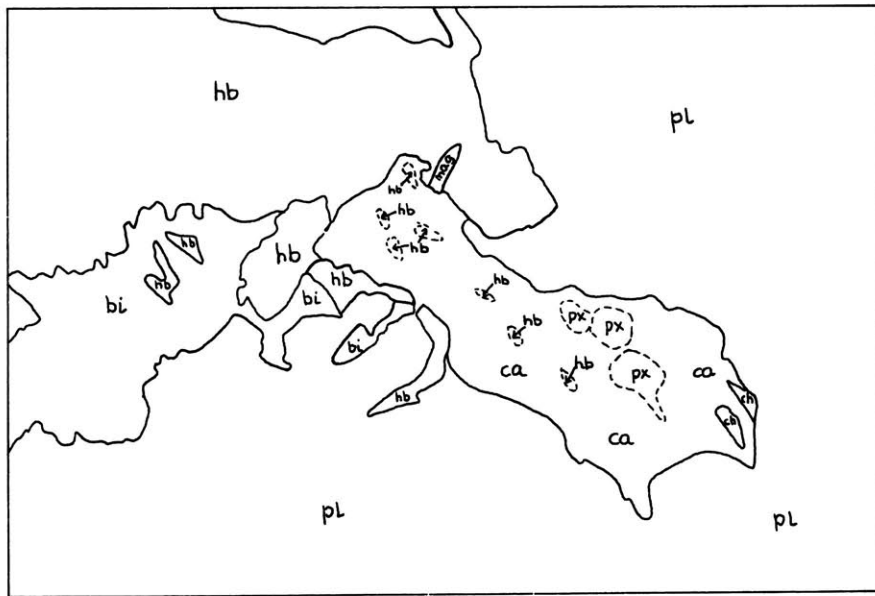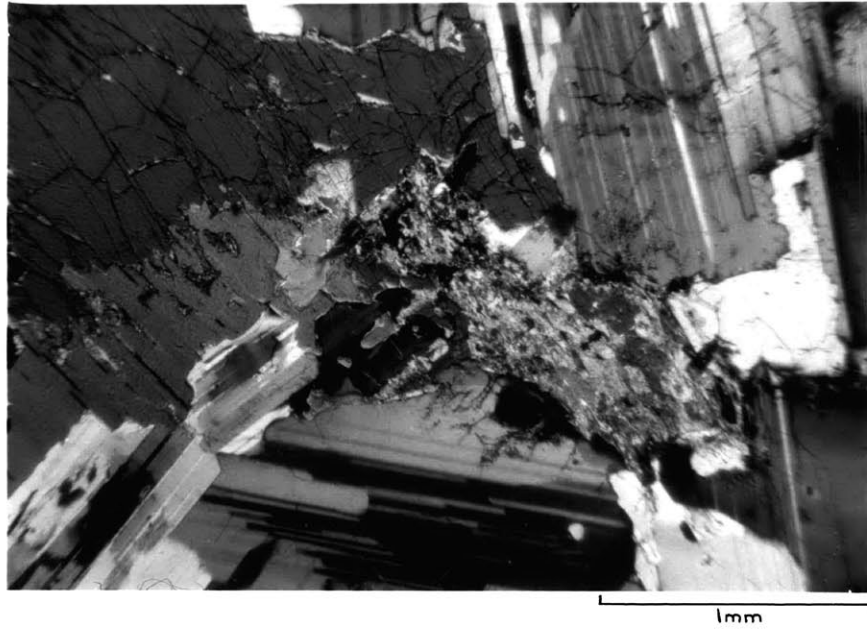
Figure 15. Pyroxene altering to carbonate, hornblende and chlorite ; and possibly hornblende altering to biotite.
Section 4-6. Cross nicols. x 36.
(pl = plagioclase ; px = pyroxene ; hb = hornblende ; bi = biotite ; mag = magnetite ; ca = carbonate ; ch = chlorite)
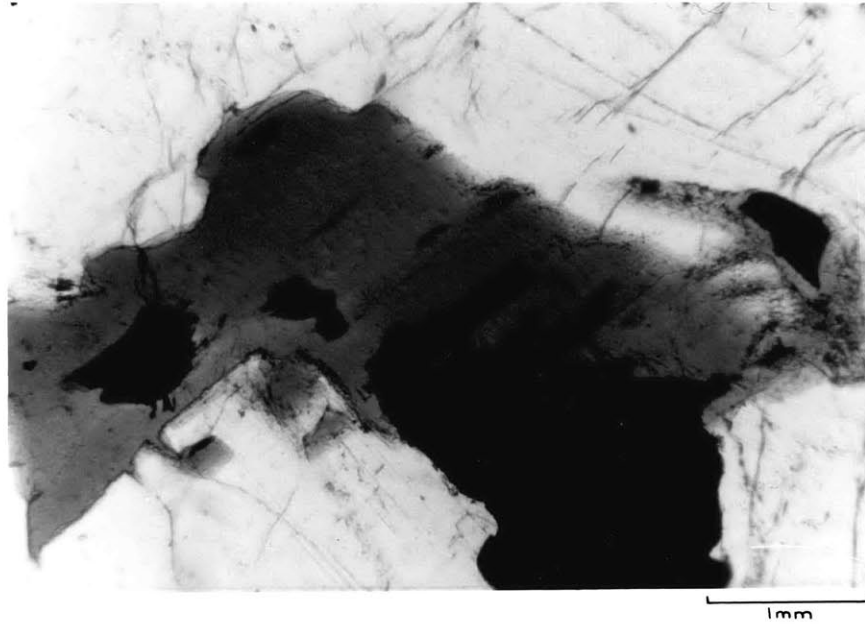
Figure 16. Biotite altering to magnetite by exsolution along {001} cleavage planes. Section 14. Ordinary light. x 138

2. Variations in mineralogical composition.

Variations in the mineralogical composition of light and dark layers, and across the discontinuity, were investigated using the method of point counting. Selected thin sections from core samples 3 and 4, and sections 7 through 15, were analyzed. The sections from core 3 and 4 were chosen so as to be oriented parallel to the layering, thus ensuring their representation of a single layer. For each of these sections, between 7,000 and 9,000 points were counted, forming a rectangular grid at intervals of 0.4mm along the length of the section and 0.2mm across it. This number of points is estimated to give a standard deviation of about 0.5% (see Chayes, 1956; p. 39). In cases where alteration of a mineral has occurred, the parent mineral is counted whenever alteration is sufficiently incomplete for it to be recognizable. Percentages of calcite and chlorite thus represent cases for which alteration is complete and the parent mineral unrecognizable. Section 7 was stained, using sodium cobaltinitrate, to reveal the orthoclase present. The results of these analyses are presented in Table 3, and in Figures 17 and 18, and will be discussed in a later section.

3. Variation in properties of individual minerals.

(i) Pyroxene

Brown (1960) has described the effect of ion substitution on the unit-cell dimensions of clinopyroxenes from the Skaergaard Instusion, East Greenland, and shown a linear dependence of the dimensions b and asinβ upon substitution of Fe^{2+} and Mg^{2+} for Ca^{2+}. A sufficiently precise measurement of these parameters for the Cape Neddick clinopyroxenes should thus reveal any significant variations in their composition.

In order to estimate the precision required, the effect of change in the 'b' cell dimension on the 221 reflection was taken as an example. Calculation showed that in this case a change of 0.02Å in the cell dimension would produce a change

Table 3. Mineralogical compositions (volume %) of selected samples.

Sample	Plag.	Px.	Biot.	Hb.	Opaq.	Apat.	Qz.	Or.	Calc.	Chl.	Serp.	Total
3-1	70.62	16.39	2.62	3.09	4.34	0.80	0.04	0.07	0.60	0.62	0.80	99.99
3-3	65.79	15.01	3.81	4.87	7.77	0.45	0.06	0.01	0.65	0.78	0.79	99.99
3-5	69.57	11.27	6.17	5.71	5.09	0.72	0.26	0.10	0.36	0.63	0.11	99.99
3-7	67.48	15.83	2.24	6.06	6.81	0.19	0.07	0.05	0.78	0.32	0.16	99.99
3-9	66.13	18.74	1.52	7.10	4.71	0.08	0.88	0.00	0.62	0.17	0.04	99.99
4-3	72.23	7.08	4.73	9.27	4.43	0.51	0.09	0.12	0.69	0.85	0.00	100.00
4-5	79.74	8.86	3.32	1.82	4.33	0.13	0.31	0.12	0.62	0.76	0.00	100.01
4-7	70.26	11.79	3.66	7.42	4.08	0.49	0.14	0.06	0.78	1.31	0.00	99.99
4-9	84.19	6.60	1.90	0.65	4.59	0.17	0.06	0.04	0.75	1.04	0.00	99.99
7	83.04	0.35	4.63	0.00	3.17	0.83	2.28	4.03	1.16	0.50	0.00	99.99
8	75.51	9.26	4.45	3.46	4.20	0.30	0.67	0.30	1.21	0.65	0.00	100.01
9	62.86	16.82	4.67	8.21	5.38	0.18	0.16	0.14	1.15	0.42	0.00	99.99
10	80.78	5.93	4.44	1.93	3.78	0.29	0.17	0.11	1.47	1.10	0.00	100.00
11	65.31	16.56	4.29	4.33	6.28	0.54	0.22	0.16	1.53	0.77	0.00	99.99
12	76.50	10.32	3.44	0.78	6.45	0.31	0.08	0.08	0.97	0.69	0.37	99.99
13	59.70	15.99	3.20	8.10	11.76	0.20	0.04	0.05	0.34	0.28	0.34	100.00
14	75.03	13.49	4.12	0.13	5.05	0.27	0.16	0.21	0.82	0.43	0.29	100.00
15	68.39	14.00	3.77	7.13	5.20	0.06	0.29	0.06	0.48	0.56	0.06	100.00
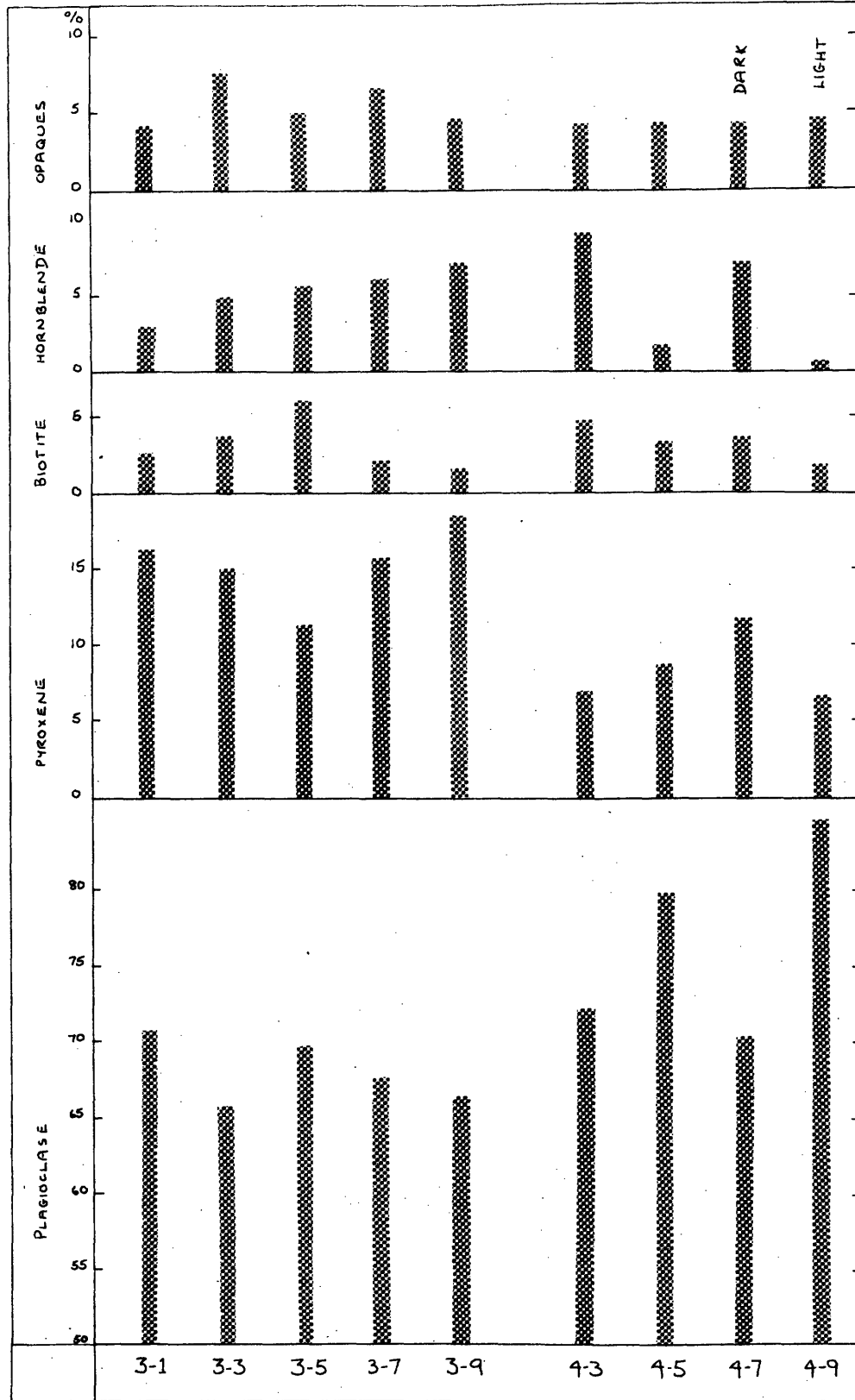
Figure 17. Variation in mineralogical composition along core samples # 3 and 4. Light and dark layers indicated where these are distinguishable on the specimen.
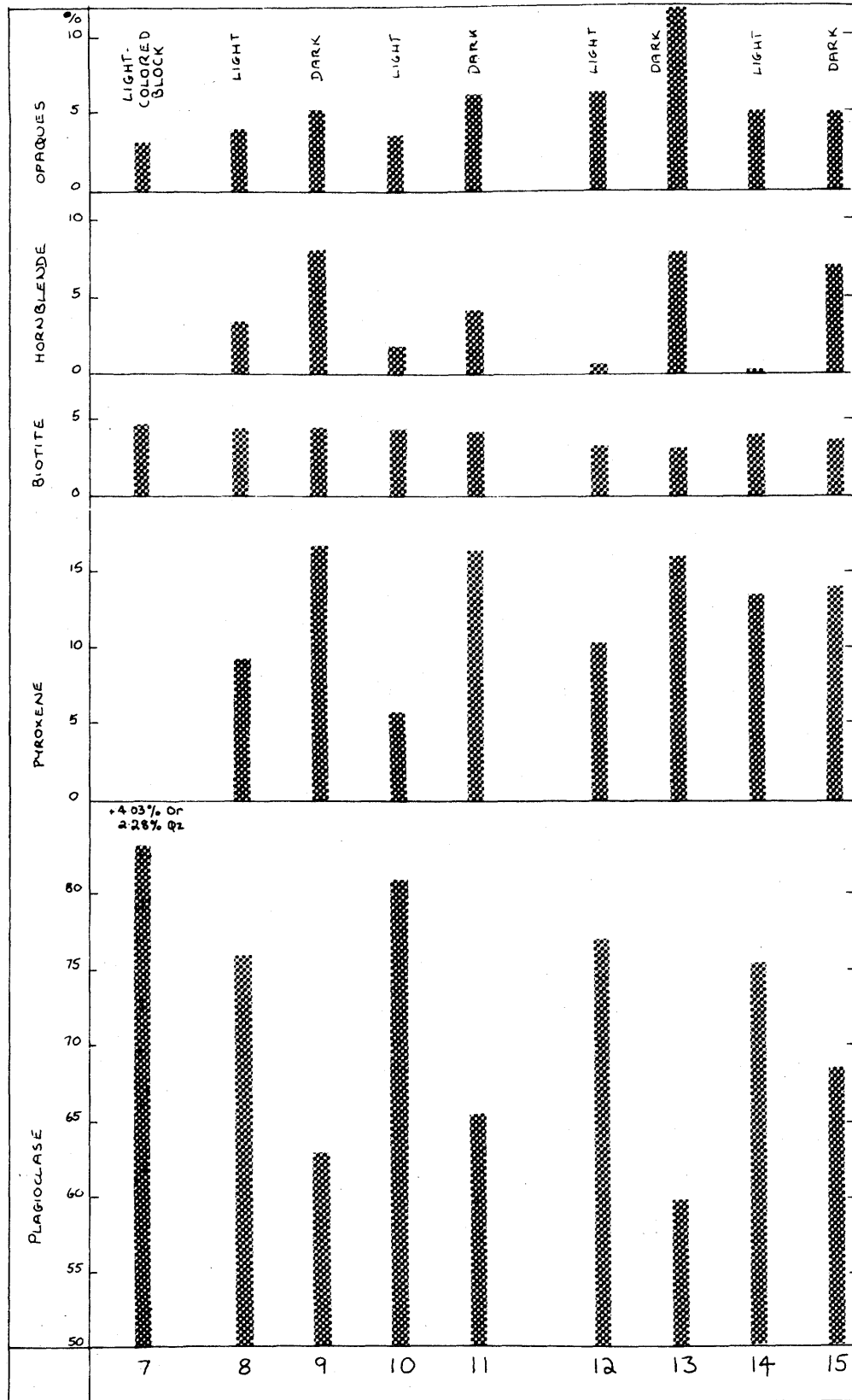
Figure 18. Mineralogical compositions of samples 7-15. Light and dark bands, as observed on the outcrop, are indicated.

of 0.02° in the diffraction angle (2θ). This is near the
limit of precision of the techniques available for diffraction
angle measurement. The accuracy may, however, be improved
by measuring several reflections and computing unit-cell
parameters which give the best fit to the entire set of
measurements. A rough estimation showed that if 10 reflec-
tions are measured, each to a precision of 0.02°, the best
fitting values of the cell parameters should be within 0.01Å
of the true values. Any variation greater than this should
therefore be detectable. Cell parameters were calculated
using a computer program written by Evans, Appelman and
Handwerker (1963). The imput for this program is a set of
measured values of 2θ, a set of approximately known cell
parameters, and the crystal system and space group. The
program compares the measured 2θ values with those computed
from the approximate cell parameters, and uses the differences
to compute a more accurate set of parameters. In several
successive cycles it provides a set of parameters from which
the computed values of 2θ give the best (least-squares) fit to
the measured values. The differences in these values are
used to compute standard deviations in these parameters. A
sample of the computer output is shown in Figure 19.

Pyroxene grains were hand sorted, under a low-power
microscope, from samples 3A - 3F, 4B - 4E and 8 - 15 as
shown in Figure 5, and ground under acetone to prepare powder
mounts for x-ray diffraction analysis. (Samples 4A and 7 con-
tained so little pyroxene that it was impossible to separate
sufficient to prepare a powder mount.)

Reflections from samples 3A - 3F and 4B - 4E were recorded
using a Guinier fine-focussing camera. Samples 8 - 15 were
analysed using a Picker diffractometer, owing to loss of
availability of the Guinier equipment. All x-ray measurements
were made using CuKα, radiation with nickel filter, at 38 Kv
and 18 ma.

The arrangement of the Guinier camera permits simultaneous
analysis of four samples, mounted on a four-port sample holder.
It is found, however, that each of the ports tends to have

	A	B	C	ALPHA	BETA	GAMMA	VOLUME
RECIPROCAL CELL	0.10672927E 00	0.11213994E 00	0.19760913E 00	90 0.0	73 55.609	90 0.0	0.22726515E-02
R C CORRECTIONS	-0.36535184E-07	0.32906632E-07	0.14514487E-07	0.0	0.004	0.0	-0.69849193E-09
DIRECT CELL	0.97506695E 01	0.89174318E 01	0.52663651E 01	90 0.0	106 4.387	90 0.0	0.44001465E 03
D C CORRECTIONS	0.28610229E-05	-0.19073486E-05	-0.95367432E-06	0.0	0.0	0.0	0.24414062E-03

LARGEST RESIDUAL REDUCED TO UNIT WEIGHT-0.02347   OBS   2   STANDARD ERROR UNIT WT OBS 0.01597   DEGREES OF FREEDOM   7

| R C STNDRD ERRS | 0.38273341E-04 | 0.50549497E-04 | 0.64207139E-04 | 0.0 | 2.067 | 0.0 | |

DIRECT CELL VARIANCE-COVARIANCE MATRIX

					ROW
0.15064554E-04	-0.82094821E-05	0.14611478E-05	0.0	0.10129788E-05	0.0	1
-0.82094830E-05	0.16158170E-04	-0.36684109E-05	0.0	-0.94197372E-06	0.0	2
0.14611460E-05	-0.36684150E-05	0.47789963E-05	0.0	0.88421245E-06	0.0	3
0.0	0.0	0.0	0.0	0.0	0.0	4
0.10129788E-05	-0.94197378E-06	0.88421245E-06	0.0	0.36152954E-06	0.0	5
0.0	0.0	0.0	0.0	0.0	0.0	6

| D C STNDRD ERRS | 0.38813083E-02 | 0.40197223E-02 | 0.21860916E-02 | 0.0 | 2.067 | 0.0 | 0.18671978E 00 |

CAPE NEDDICK PYROXENE   C4-E   3-1   HKL LISTING - *** REFERS TO FIXED, R TO REJECTS MONOC

N	H	K	L	D CALC	D OBS	LAMBDA	2-THETA CALC	2-THETA OBS	2-THETA DIFF	WEIGHT
1	1	1	0	6.459483		1.540500	13.69666			
2	2	0	0	4.684749		1.540500	18.92667			
3	0	2	0	4.458715		1.540500	19.89566			
4	-1	1	1	4.413503		1.540500	20.10159			
5	1	1	1	3.658947		1.540500	24.30463			
6	0	2	1	3.345422		1.540500	26.62239			
***	0	2	1	3.345422	3.347941	1.540500	26.62239	26.6020	0.02040	1.00000
7	2	2	0	3.229741		1.540500	27.59447			
***	2	2	0	3.229741	3.232437	1.540500	27.59447	27.5710	0.02347	1.00000
8	-2	2	1	2.993980		1.540500	29.81581			
***	-2	2	1	2.993980	2.995141	1.540500	29.81581	29.8040	0.01184	1.00000
9	3	1	0	2.947614		1.540500	30.29594			
***	3	1	0	2.947614	2.947515	1.540500	30.29594	30.2970	-0.00104	1.00000
10	-3	1	1	2.897523		1.540500	30.83261			
***	-3	1	1	2.897523	2.897671	1.540500	30.83261	30.8310	0.00163	1.00000
11	1	3	0	2.833311		1.540500	31.54935			
12	-1	3	1	2.565451		1.540500	34.94397			
***	-1	3	1	2.565451	2.564596	1.540500	34.94397	34.9560	-0.01202	1.00000
13	-2	0	2	2.539611		1.540500	35.31116			
14	0	0	2	2.530248		1.540500	35.44614			
***	0	0	2	2.530248	2.530742	1.540500	35.44614	35.4390	0.00714	1.00000
15	-1	1	2	2.525327		1.540500	35.51752			
16	2	2	1	2.513607		1.540500	35.68866			
***	2	2	1	2.513607	2.513313	1.540500	35.68866	35.6930	-0.00433	1.00000
17	1	3	1	2.388430		1.540500	37.62741			
18	4	0	0	2.342374		1.540500	38.39590			
19	3	1	1	2.299120		1.540500	39.14743			
***	3	1	1	2.299120	2.299146	1.540500	39.14743	39.1470	0.00046	1.00000
20	0	4	0	2.229357		1.540500	40.42502			
21	-3	1	2	2.229268		1.540500	40.42670			
22	1	1	2	2.216641		1.540500	40.66711			
***	1	1	2	2.216641	2.216075	1.540500	40.66711	40.6780	-0.01086	1.00000
23	-2	2	2	2.206752		1.540500	40.85751			
24	0	2	2	2.200601		1.540500	40.97684			
25	3	3	0	2.153161		1.540500	41.92166			
26	-3	3	1	2.133402		1.540500	42.32852			
***	-3	3	1	2.133402	2.132514	1.540500	42.32852	42.3470	-0.01846	1.00000
27	-4	2	1	2.108677		1.540500	42.84918			
28	4	2	0	2.073637		1.540500	43.60999			
29	0	4	1	2.040157		1.540500	44.36331			
30	-4	0	2	2.020191		1.540500	44.82544			
31	2	4	0	2.013045		1.540500	44.99329			
32	2	0	2	2.006124		1.540500	45.15707			
33	-1	3	2	1.971004		1.540500	46.00739			
34	-2	4	1	1.951939		1.540500	46.48300			
35	-5	1	1	1.896571		1.540500	47.92361			
36	3	3	1	1.857647		1.540500	48.99298			
37	-4	2	2	1.840123		1.540500	49.49069			
38	5	1	0	1.833847		1.540500	49.67151			
39	2	2	2	1.829473		1.540500	49.79837			

Figure 19. Sample of computer output for least-squares refinement of pyroxene cell parameters.

slightly different focussing characteristics, thus for con-
sistency each sample was allotted to a separate sample holder
and mounted in the two center ports. Synthetic spinel
($MgAl_2O_4$, a_o = 8.0833), provided by W. C. Luth, was used as
an internal standard. The Guinier camera records the dif-
fraction pattern on photographic film as a series of dark
lines, the geometry of the arrangement being such that a
separation of 1mm on the film corresponds to a difference
of $\frac{1}{2}°$ in diffraction angle. In theory, it should be possible
to measure line separations to an accuracy of 0.01mm, and
thus obtain 2θ to an accuracy of 0.005°. In practise, however,
the focussing characteristics of the camera and the finite
width of diffraction lines introduce instrumental and per-
sonal errors which reduce the accuracy. By mounting the same
sample in different ports of the sample holder, and by making
two series of measurements on each port, it was hoped to
locate and estimate these errors. In order to make comparison
between samples as close as possible, reflections having
fixed indices were used. Eleven reflections, which appeared
as reasonably strong and sharp lines on each film, were
selected for the least-squares refinement: 021 220 $\bar{2}$21
310 $\bar{3}$11 $\bar{1}$31 002 221 311 112 $\bar{3}$31. The results of the
Guinier refinement are presented in Tables 4 and 5, and in
Figures 20a and 21a. Results from samples 4B and 4C are
missing due to inadequate quality of the films obtained.

Powdered pyroxene from samples 8 - 15 was mixed with acetone
and prepared for diffractometer analysis as a smear mount on
a glass microscope slide. In order that personal and in-
strumental errors might be located, each sample was run
twice, once as 2θ was increased from 0 to 70°, and again
as 2θ was decreased through the same range. Twelve dif-
fraction peaks, which showed up reasonably strongly and
sharply on each of the recordings, were used in the least-
squares refinement: 021 220 $\bar{2}$21 310 $\bar{3}$11 $\bar{1}$31 221 311
330 $\bar{3}$31 $\bar{4}$21 and 150. The results of the diffractometer
refinement are presented in Table 6 and in Figures 20b and
21b. It may be noted, from Figures 20 and 21, that although

Table 4. Unit-cell dimensions of pyroxenes from samples 3-A - 3-E. Measurements using Guinier fine-focussing camera.

		a	Δ a	b	Δ b	c	Δ c
3-A	i*	9.751	0.005	8.943	0.005	5.255	0.003
	ii	9.755	0.005	8.933	0.005	5.257	0.003
	iii	9.759	0.005	8.934	0.005	5.258	0.003
	iv	9.761	0.002	8.938	0.002	5.260	0.001
3-B	i	9.760	0.003	8.917	0.003	5.265	0.002
	ii	9.755	0.003	8.921	0.003	5.264	0.002
	iii	9.756	0.002	8.920	0.002	5.267	0.001
	iv	9.751	0.003	8.921	0.003	5.265	0.001
3-C	i	9.758	0.008	8.915	0.008	5.258	0.004
	ii	9.756	0.005	8.915	0.005	5.261	0.003
	iii	9.749	0.005	8.923	0.005	5.261	0.003
	iv	9.754	0.004	8.921	0.004	5.263	0.002
3-D	i	9.749	0.002	8.921	0.002	5.263	0.001
	ii	9.751	0.003	8.914	0.004	5.265	0.002
	iii	9.748	0.003	8.919	0.003	5.268	0.002
	iv	9.754	0.003	8.921	0.003	5.267	0.002
3-E	i	9.751	0.003	8.928	0.003	5.263	0.002
	ii	9.755	0.003	8.924	0.003	5.264	0.002
	iii	9.751	0.002	8.918	0.002	5.263	0.001
	iv	9.760	0.004	8.919	0.004	5.260	0.002

*Four series of measurements for each sample are represented as follows:
 i   First series of measurements on port #2 of Guinier mount
 ii   Second series of measurements on port #2 of Guinier mount
 iii First series of measurements on port #3 of Guinier mount
 iv   Second series of measurements on port #3 of Guinier mount

Table 4. Unit-cell dimensions of pyroxenes from samples 3-A - 3-E.   (Continued)

		sinβ	Δsinβ	asinβ	Δ(asinβ)	V	ΔV
3-A	i*	106° 4.1'	2.5'	9.370	0.007	440.36	0.23
	ii	106° 5.5'	2.4'	9.373	0.007	440.18	0.23
	iii	106° 0.1'	2.7'	9.381	0.007	440.68	0.24
	iv	106° 2.8'	1.0'	9.381	0.003	440.98	0.09
3-B	i	106° 5.6'	1.8'	9.378	0.004	440.11	0.16
	ii	106° 5.4'	1.8'	9.373	0.004	440.20	0.16
	iii	106° 6.7'	1.2'	9.373	0.004	440.28	0.11
	iv	106° 4.7'	1.3'	9.370	0.004	440.06	0.12
3-C	i	105°59.8'	4.2'	9.380	0.010	439.75	0.38
	ii	106° 1.5'	2.6'	9.377	0.007	439.75	0.24
	iii	106° 2.2'	2.8'	9.370	0.008	439.85	0.25
	iv	106° 3.7'	1.9'	9.373	0.005	440.11	0.18
3-D	i	106° 5.1'	1.2'	9.367	0.003	439.80	0.11
	ii	106° 8.6'	1.8'	9.367	0.004	439.59	0.16
	iii	106° 7.9'	1.6'	9.364	0.004	439.95	0.14
	iv	106° 7.8'	1.7'	9.370	0.004	440.24	0.15
3-E	i	106° 4.1'	1.5'	9.370	0.004	440.28	0.14
	ii	106° 6.7'	1.7'	9.372	0.004	440.21	0.15
	iii	106° 3.3'	0.8'	9.371	0.003	439.85	0.08
	iv	106° 2.1'	2.2'	9.380	0.006	440.05	0.20

*Four series of measurements for each sample are represented as follows:
     i   First series of measurements on port #2 of Guinier mount
     ii   Second series of measurements on port #2 of Guinier mount
     iii   First series of measurements on port #3 of Guinier mount
     iv   Second series of measurements on port #3 of Guinier mount

Table 5. Unit-cell dimensions of pyroxenes from samples 4-D and 4-E. Measurements
using Guinier fine-focussing camera.

		a	Δ a	b	Δ b	c	Δ c
4-D	i*	9.752	0.003	8.918	0.003	5.266	0.001
	ii	9.753	0.002	8.917	0.002	5.267	0.001
	iii	9.755	0.003	8.915	0.003	5.267	0.002
	iv	9.757	0.003	8.916	0.003	5.267	0.002
4-E	i	9.756	0.004	8.916	0.004	5.271	0.002
	ii	9.762	0.004	8.910	0.004	5.273	0.002
	iii	9.751	0.004	8.917	0.004	5.266	0.002
	iv	9.754	0.003	8.918	0.003	5.268	0.002

*Four series of measurements for each sample are represented as follows:
    i   First series of measurements on port #2 of Guinier mount
    ii   Second series of measurements on port #2 of Guinier mount
    iii   First series of measurements on port #3 of Guinier mount
    iv   Second series of measurements on port #3 of Guinier mount

Table 5. Unit-cell dimensions of pyroxenes from sample 4-D and 4-E. Measurements using Guinier fine-focussing camera. (Continued)

		$\sin\beta$	$\Delta\sin\beta$	$a\sin\beta$	$\Delta(a\sin\beta)$	V	ΔV
4-D	i*	106° 4.9'	1.4'	9.370	0.004	440.01	0.12
	ii	106° 6.4'	1.1'	9.370	0.003	440.02	0.10
	iii	106° 5.3'	1.4'	9.373	0.004	440.16	0.13
	iv	106° 6.1'	1.7'	9.374	0.004	440.27	0.15
4-E	i	106° 5.6'	2.1'	9.374	0.005	440.53	0.19
	ii	106° 9.0'	2.0'	9.377	0.006	440.53	0.18
	iii	106! 4.4'	2.1'	9.370	0.006	440.01	0.19
	iv	106° 5.6'	1.5'	9.372	0.004	440.30	0.25

*Four series of measurements for each sample are represented as follows:
    i   First series of measurements on port #2 of Guinier mount
    ii   Second series of measurements on port #2 of Guinier mount
    iii   First series of measurements on port #3 of Guinier mount
    iv   Second series of measurements on port #3 of Guinier mount

Table 6. Unit-cell dimensions of pyroxenes from samples 8 - 15. Measurements using Picker diffractometer.

		a	Δ a	b	Δ b	c	Δ c
8	i*	9.752	0.003	8.914	0.003	5.273	0.005
	ii	9.755	0.004	8.908	0.003	5.278	0.006
9	i	9.754	0.002	8.916	0.002	5.269	0.004
	ii	9.753	0.002	8.916	0.002	5.271	0.004
10	i	9.753	0.004	8.912	0.003	5.275	0.006
	ii	9.754	0.003	8.912	0.002	5.276	0.004
11	i	9.754	0.003	8.917	0.002	5.266	0.005
	ii	9.755	0.003	8.918	0.002	5.268	0.004
12	i	9.755	0.001	8.915	0.001	5.268	0.002
	ii	9.752	0.002	8.914	0.001	5.272	0.003
13	i	9.755	0.003	8.914	0.002	5.270	0.004
	ii	9.754	0.002	8.918	0.001	5.273	0.003
14	i	9.756	0.005	8.913	0.003	5.275	0.007
	ii	9.754	0.006	8.913	0.004	5.272	0.009
15	i	9.753	0.004	8.915	0.003	5.269	0.006
	ii	9.751	0.004	8.916	0.003	5.271	0.006

*Two series of measurements for each sample are represented as follows:
    i   Diffractometer run in forward direction
    ii Diffractometer run in reverse direction

(Table 6 continued on next page)

Table 6. Unit-cell dimensions of pyroxenes from sample 8 - 15. Measurements using Picker diffractometer. (Continued)

		$\sin\beta$	$\Delta\sin\beta$	$a\sin\beta$	$\Delta(a\sin\beta)$	V	ΔV
8	i	106° 2.1'	2.1'	9.373	0.005	440.54	0.35
	ii	106° 3.9'	2.4'	9.374	0.006	440.74	0.40
9	i	106° 1.3'	1.5'	9.375	0.003	440.40	0.25
	ii	106° 2.3'	1.5'	9.373	0.003	440.53	0.24
10	i	106° 3.9'	2.6'	9.372	0.006	440.60	0.42
	ii	106° 2.1'	1.7'	9.374	0.004	440.81	0.28
11	i	106° 2.3'	2.0'	9.374	0.004	440.23	0.32
	ii	106° 3.3'	1.6'	9.375	0.004	440.43	0.27
12	i	106° 3.4'	0.8'	9.374	0.002	440.26	0.13
	ii	106° 4.4'	1.0'	9.371	0.003	440.35	0.17
13	i	106° 5.0'	1.8'	9.373	0.004	440.31	0.29
	ii	106° 4.9'	1.1'	9.372	0.003	440.67	0.18
14	i	106° 6.1'	2.9'	9.373	0.007	440.70	0.47
	ii	106° 5.8'	3.6'	9.372	0.008	440.32	0.60
15	i	106° 2.8'	2.2'	9.373	0.006	440.26	0.38
	ii	106° 1.4'	2.4'	9.372	0.006	440.42	0.40

*Two series of measurements for each sample are represented as follows:
  i   Diffractometer run in forward direction
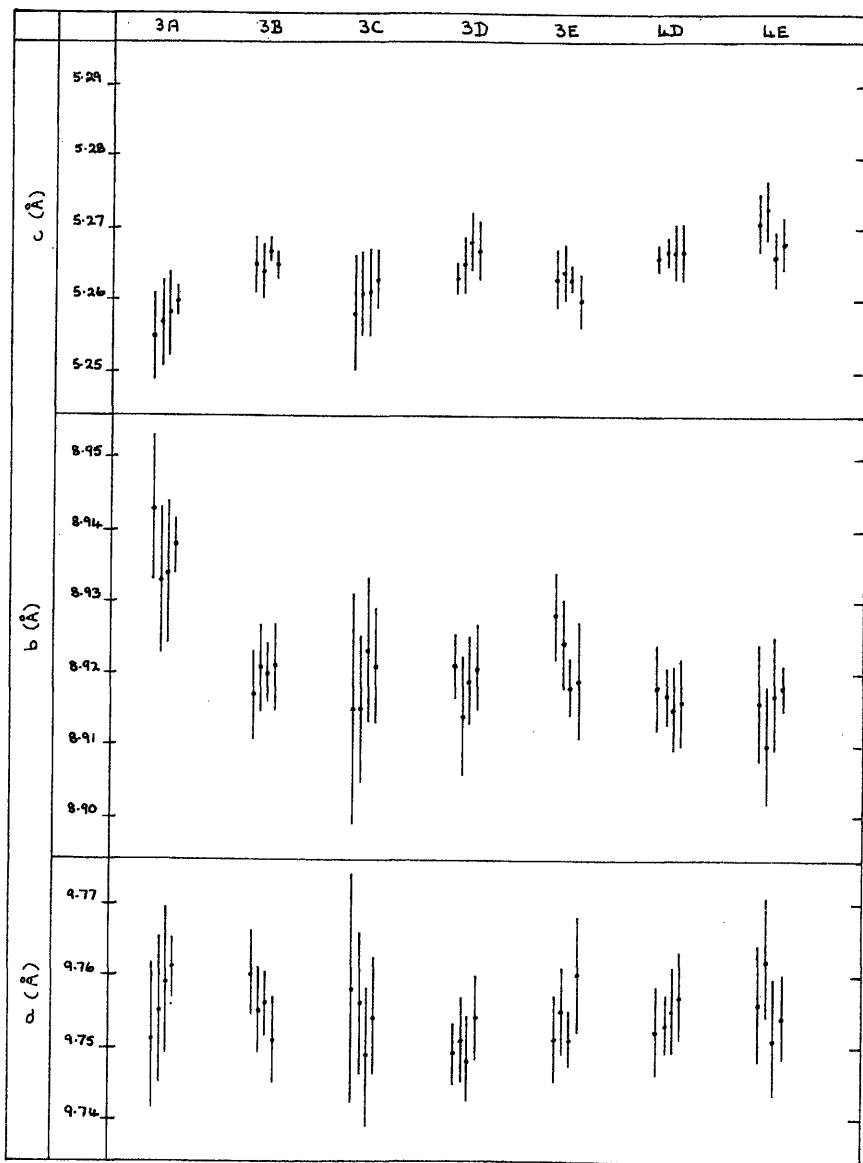 ii Diffractometer run in reverse direction

Figure 20a. Unit-cell dimensions of pyroxenes from samples 3A - 3E, 4D and 4E. Measurements using Guinier fine-focussing camera. The four sets of results for each sample represent mounts on two ports of the Guinier sample holder, and two series of measurements for each port. Vertical bars represent two computed standard deviations for each series of measurements.
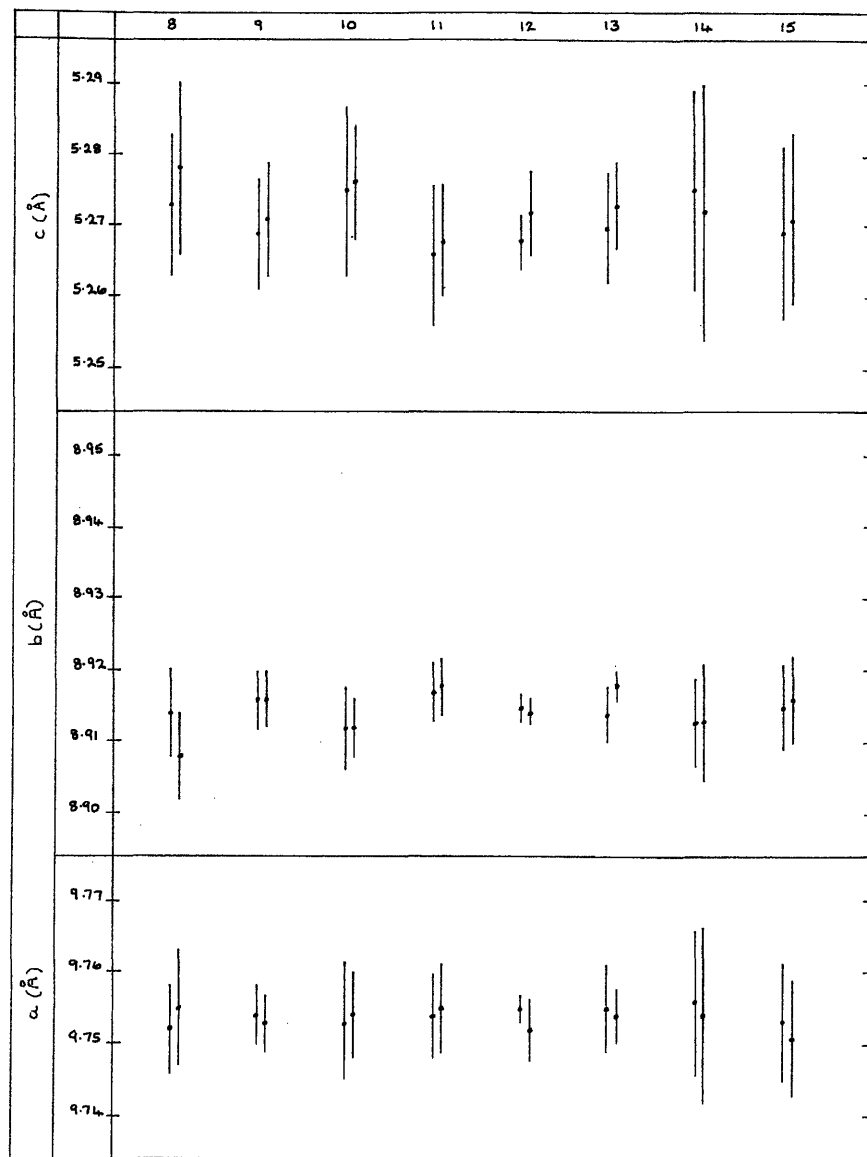
Figure 20b. Unit-cell dimensions of pyroxenes from samples 8-15. Measurements using Picker diffractometer. The two sets of results for each sample represent measurements made on forward and reversed diffractometer runs. Vertical bars represent two computed standard deviations for each series of measurements.
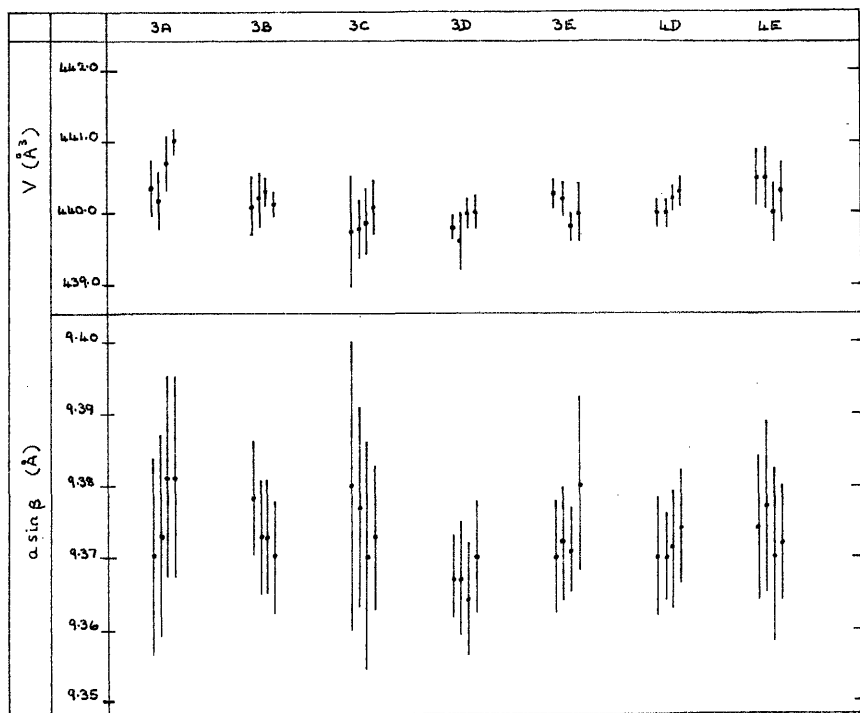
Figure 21a. Values of $a\sin\beta$ and unit cell volume (V) for pyroxenes from samples 3A-3E, 4D and 4E. Measurements using Guinier fine-focussing camera. The four sets of results for each sample represent mounts on two ports of the Guinier sample holder, and two series of measurements on each port. Vertical bars represent two computed standard deviations for each series of measurements.

Figure 21b. Values of $a\sin\beta$ and unit-cell volume (V) for pyroxenes from samples 8-15. Measurements using Picker diffractometer. The two sets of results for each sample represent measurements made on forward and reversed diffractometer runs. Vertical bars represent two computed standard deviations for each series of measurements.
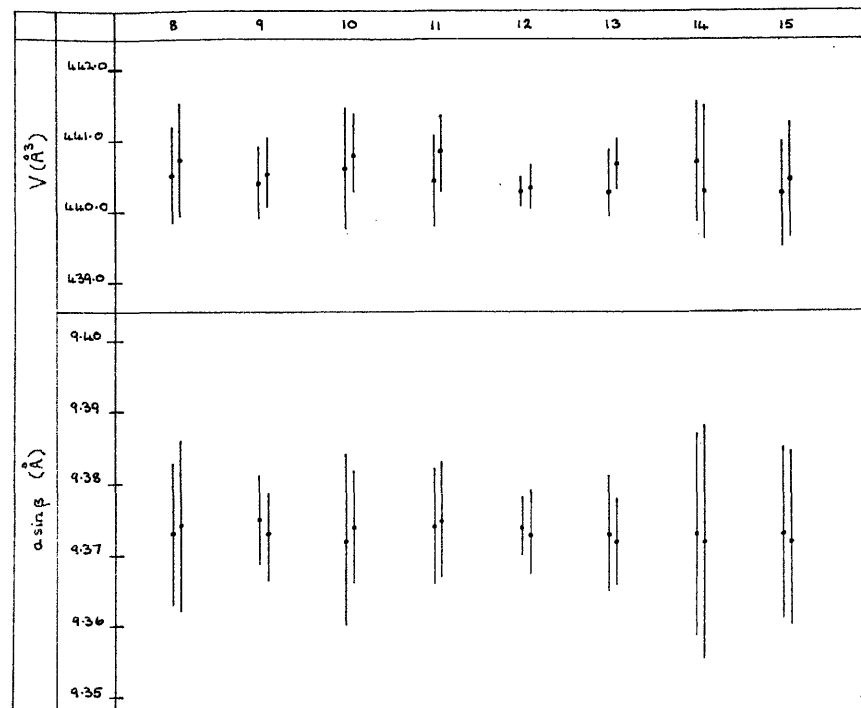
a similar range of standard deviations is obtained using either
the Guinier camera or diffractometer, better reproducibility
is generally shown in the diffractometer measurements.

(ii) Biotite and hornblende

Biotite and hornblende were examined by refractive
index measurements. The refractive index of biotite as a
function of iron content, on the join phlogopite-annite, has
been studied by Wones (1963). His data shows that an in-
crease of 1% in iron content produces an increase of about
0.001 in the γ refractive index. The relation between re-
fractive indices and chemical composition of common hornblende
is given by Deer, Howie and Zussman (1963, p. 296), and shows
that an increase of 1% in the ratio $Mg/(Mg+Fe^{+2}+Fe^{+3}+Mn)$ pro-
duces a decrease in the α and γ refractive indices of about
0.001.

Refractive index measurements were made using immersion
oils calibrated at intervals of 0.002; thus any changes of
greater than ±2% in iron or magnesium content should be de-
tectable. The measurements were made on samples 8 - 15.
For biotite, both α and γ refractive indices were measured,
the difference between β and γ indices being undetectable.
For hornblende the γ index only was measured.

The refractive indices of biotite were found to be
constant for all samples:

$$\gamma = 1.670 \pm 0.002$$
$$\alpha = 1.605 \pm 0.001 \qquad \text{at } 24°C$$

The high value of γ is indicative of high iron, high titanium,
or both (Hall, 1941b).

The hornblende index also was constant for all samples:

$$\gamma = 1.690 \pm .002 \qquad \text{at } 24°C$$

The composition cannot be determined reliably from the re-
lationship given by Deer, Howie and Zussman (1963), since
this does not take into account the effect of titanium content.

(iii) Plagioclase

The strong zoning described above makes study of
plagioclase compositions by x-ray techniques unsuitable, since
these would merely give an average composition over all the

zones of several grains. Refractive index measurements also
are unsuitable, since only the edge of a particular grain
would be determined. An attempt at petrographic study of
variation in the composition of plagioclase cores in samples
3 and 4 was made by extinction angle measurements on sections
perpendicular to the Z vibration direction. Such sections
were chosen, firstly because they revealed the most distinct
pattern of zoning and enabled specific location of the core,
and secondly because the extinction angle measured (X∧010)
is the most sensitive to variation in composition for calcic
plagioclase. Difficulty was encountered due to the extremely
irregular form of the grains, which are often so intergrown
that a particular grain is hard to define. However, several
grains sufficiently complete for cores to be determined were
found per thin section, and an idea of the range of core
compositions could thus be obtained. The results of the
measurements are presented in Table 7, together with cor-
responding core compositions obtained from Duparc and Rein-
hard (1924, p. 32). (One plagioclase grain, from core sample
1, was analysed during the electron microprobe run, and
showed 14.1% CaO, corresponding to an anorthite content of
70%).

Table 7. Composition of plagioclase cores obtained from extinction angle measurements.

Section	$X^\wedge 010$	%An	Section	$X^\wedge 010$	%An
	30.7	56		31.1	56
	33.8	61		30.5	56
3-1	38.7	69	4-1	33.4	58
	35.3	63		34.2	58
	27.7	53		33.1	60
	34.0	61		24.0	50
	41.6	74		39.0	70
3-3	37.4	66	4-3	33.7	59
	35.5	63		27.6	53
	33.1	60		34.0	61
	28.3	54		41.8	75
	31.6	58		35.2	63
3-5	33.8	59	4-5	34.0	61
	35.7	64		27.0	52
	28.9	55.5		29.3	55

Summary of Results

Paragenetic relationships between individual minerals were summarised in a previous section (1B).

Inspection of Figures 17 and 18, and Table 3, indicates the following generalizations as to the role of varying mineralogical composition in determining light and dark layers:

(i)   Plagioclase is higher in light layers than in dark layers.

(ii)   In samples 8 - 15, pyroxene is higher in dark layers than in light layers. In sample 4, however, this does not appear to hold.

(iii)   Biotite is fairly constant in all samples, and whatever variability it does show does not appear to correlate significantly with the nature of the layers.

(iv)   Hornblende is considerably higher in dark layers; in light layers it is present only in very small amounts.

(v)   The proportion of opaque minerals does not appear to correlate significantly with the nature of the layers.

(vi)   As far as can be judged from the small amounts in which they occur, minor constituents have no significant correlation with the layering.

(vii)   The light-colored block (sample 7) is rich in quartz and orthoclase, and poor in pyroxene and hornblende, compared to all the other samples.
Core sample 3 showed remarkably few variations, none of which appeared to be significant or correlative. This explains the difficulty encountered in distinguishing layering in the sample, but is unexpected on account of the layering observed on the outcrop. The only detectable variations are slight fluctuations in the proportion of plagioclase, of dark minerals as a whole, and of opaque minerals.

Estimation of the significance of variations on either side of the discontinuity can only be subjective. It seems to the author that, on the eastern side of the discontinuity, (samples 4 and 8-11), fluctuations are slightly more marked,

and the proportion of plagioclase in either type of layer is
higher, than on the western side. There is, however, one
variation that is believed to have real significance, and
that is in the amount of serpentine present. The results
of point counting, as shown in Table 3, show zero serpentine
for all sections from core sample 4, and for sections 8 - 11.
These samples are all from the eastern side of the discontinuity.
The sections from core sample 3, however, and sections 12 - 15,
all of which are from the western side of the discontinuity,
all show some serpentine, and generally in significant quantity.
In order to check the reality of this variation the thin
sections were re-examined and a count made of the number of
serpentine aggregates occurring in each. The results of this
count are presented in Table 8. The few aggregates observed
in thin sections from the eastern side of the discontinuity
are in all cases very tiny; those on the western side are
numerous and generally large, usually greater than 1mm, and
sometimes greater than 2mm, in length.

The only detectable variation in the properties of
individual minerals is in the pyroxenes. Hornblende and
biotite, if they vary, do so by less than 0.02%. Further
investigation, however, using x-ray analysis, may reveal vari-
ations since this method proves to be more sensitive as shown
below in the case of pyroxenes. Plagioclase compositions
vary too much within a single thin section to enable varia-
tions between thin sections to be revealed.

The pyroxene compositions are plotted in Figure 22,
which is based on that of Brown (1960). In this plot the
values of all measurements on each sample have been averaged,
thus the points plotted actually have an area of uncertainty
around them. For clarity these areas are not shown on the
diagram, and it is believed that the trends shown by the
points themselves are significant. These trends are as
follows:

(i) Pyroxenes from dark bands (samples 9, 11, 13, 15,
4D) are richer in iron (by an order of about 2%) than those
from light bands.

Table 8. Occurrence of serpentine aggregates.

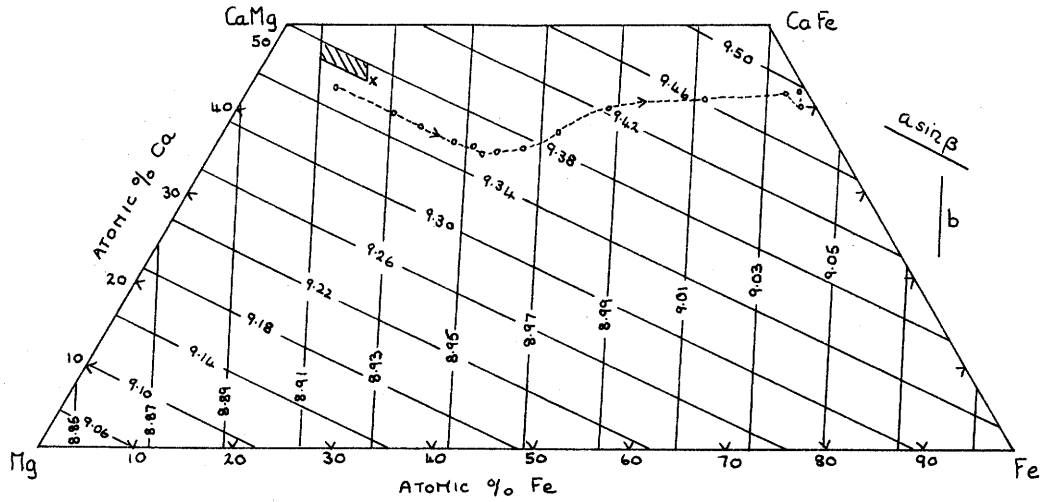| West of discontinuity		East of discontinuity	
Thin section #	No. of serpentine aggregates	Thin section #	No. of serpentine aggregates
3-1	12	4-2	1 (<0.5mm)
3-2	10	4-3	0
3-3	11	4-4	1 (<0.5mm)
3-4	14	4-5	0
3-5	3	4-6	1 (<0.5mm)
3-6	2	4-7	0
3-7	2	4-8	1 (<0.5mm)
3-8	2	4-9	0
3-9	1		
		7-1	0
12	2	8	0
13	2	9	1 (<0.5mm)
14	3	10	0
15	1	11	0

Figure 22 a. Variation in b and a sin β in the common clinopyroxene trapezium, after Brown (1960). The shaded area represents the general region of values obtained for Cape Neddick clinopyroxenes, shown in detail below. 'X' indicates the composition of the Cape Neddick clinopyroxene which was analysed by electron microprobe. Compositions of clinopyroxenes from the layered series of the Skaergaard intrusion, East Greenland, are shown for comparison (circles), and their trend of differentiation by the broken line (after Wager and Brown, 1967).
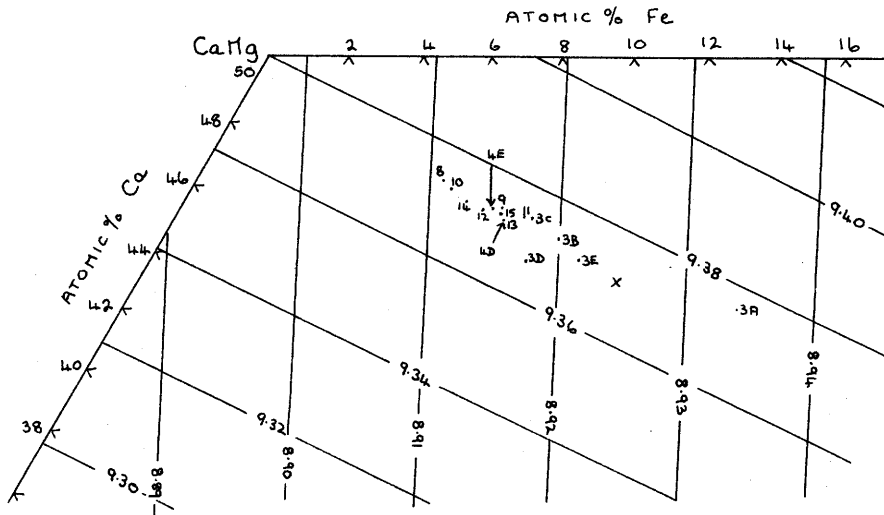

Figure 22b. Enlargement of part of figure 22 a, showing the compositions of Cape Neddick clinopyroxenes as determined by measurements of b and a sin β (averaged values used) 'X' indicates the composition of the clinopyroxene that was analysed by electron microprobe.

(ii)   Pyroxenes from the eastern side of the discontinuity
(8, 9, 10, 11 and 4E; not, however, 4D) tend to be very slightly
more calcic (by an order of about 0.5%) than those from the
western side.

Pyroxenes from core sample 3 show a wide range of variability.
It must be left to the judgement of the reader to decide
whether such variability in one sample renders the trends out-
lined above as merely coincidental. The author, however be-
lieves that the trends are real and that the extreme varia-
tion in core sample 3 is anomalous.

The c dimension varies somewhat irregularly. The ion
substitution that would effect variation in this direction,
that is, in the direction of the chains of silica tetrahedra,
would be Al^{3+} for Ca^{4+}. This may be the case; however Brown
(1960) noticed a similar irregular variation in the c dimen-
sion of clinopyroxenes from the Skaergaard Intrusion and sug-
gested that it might be related to exsolution. If so, the
same may apply to Cape Neddick clinopyroxenes, the oriented
inclusions described in an earlier section being exsolution
lamellae.

Discussion of Results

Petrogenesis

In all sections it appears that plagioclase crystallized
prior to pyroxene, and pyroxene prior to hornblende. Biotite
presents a problem, since it is present both in plagioclase
cores and plagioclase interstices. This implies that, al-
though the majority of biotite crystallised late, a small
amount of it was in fact the earliest crystalline phase.

The paragenesis is complicated by the irregular forms and
patchy growth of the plagioclase. Comparison with photomicro-
graphs of plagioclase phenocrysts erupted from Kilauea volcano,
Hawaii (Richter and Murata (1966), p. D9) indicates that they
have undergone considerable resorption and recrystallization.
Possibly early formed crystals have been brought into contact
with fresh supplies of magma as a result of movement either
of the crystals themselves, the magma, or both. The greater
part of this irregular crystallization appears to have taken
place before that of the ferromagnesian minerals, which always
occur between the more euhedral edges of plagioclase grains.
These edges presumably represent the latest stage of plagio-
clase crystallization.

Magnetite, since it is observed within every other phase,
has crystallized from the earliest stages, as well as being
a product of exsolution from biotite. Carbonate represents
late magmatic alteration of ferromagnesian minerals. Apatite
has its common role as an accessory mineral of middle-to-late
stage crystallization.

Serpentine, from the characteristic, rounded form of its
aggregates and the irregular fracturing observed, is assumed
to be pseudomorphic after olivine. It is in various stages
of alteration to carbonate. Where serpentine is observed
it appears that olivine must have been the first ferromagnesian
mineral to crystallize, since it is always wholly or partially
surrounded by pyroxene or hornblende.

Quartz and orthoclase are the products of the latest, silica rich melt. Orthoclase is often observed close to biotite and magnetite, and may be a product of biotite-magnetite exsolution. Figure 23 shows the inferred paragenesis.

Origin of Layering

Most theories of layering in basic rocks invoke gravity to promote differentiation and some kind of periodic motion of the magma to produce cyclic deposition. Hess (1960) suggests that the layered series of the Stillwater complex, Montana, results from variable rates of accumulation of crystals of different density as these fall in ascending and decending convection currents. Jackson (1961) describes a gravity/convection-current mechanism for the layering in the ultramafic zone of the Stillwater complex. Here the change in mineralogy of settled crystals is due to convective overturn in the top half of the magma chamber and stable conditions at the bottom. Wager (1953) suggests that the layered series of the Skaergaard intrusion, East Greenland, is caused by variation in velocity of the convection currents moving across the floor of the magma pool. Heavier crystals are deposited while the velocity is higher, lighter crystals while it is lower. He later (1959) considers the possibility of a process involving alternate supersaturation and nucleation, combined with convection currents, in controlling the layering.

Brown (1956) explains layering in the Rhum intrusion, Outer Hebrides, as resulting from periodic fresh influxes of magma. He suggests that the intrusion was connected with an overlying volcano, and periods of volcanic eruption produced changes in physical and chemical conditions (particularly temperature and water content) which determine the crystallizing phase. As erupted magma left the chamber fresh supplies came in from below and a new cycle commenced. Lombaard (1934) also favors an intermittent magma supply as controlling factor in the layered series of the Bushveld complex, South Africa.
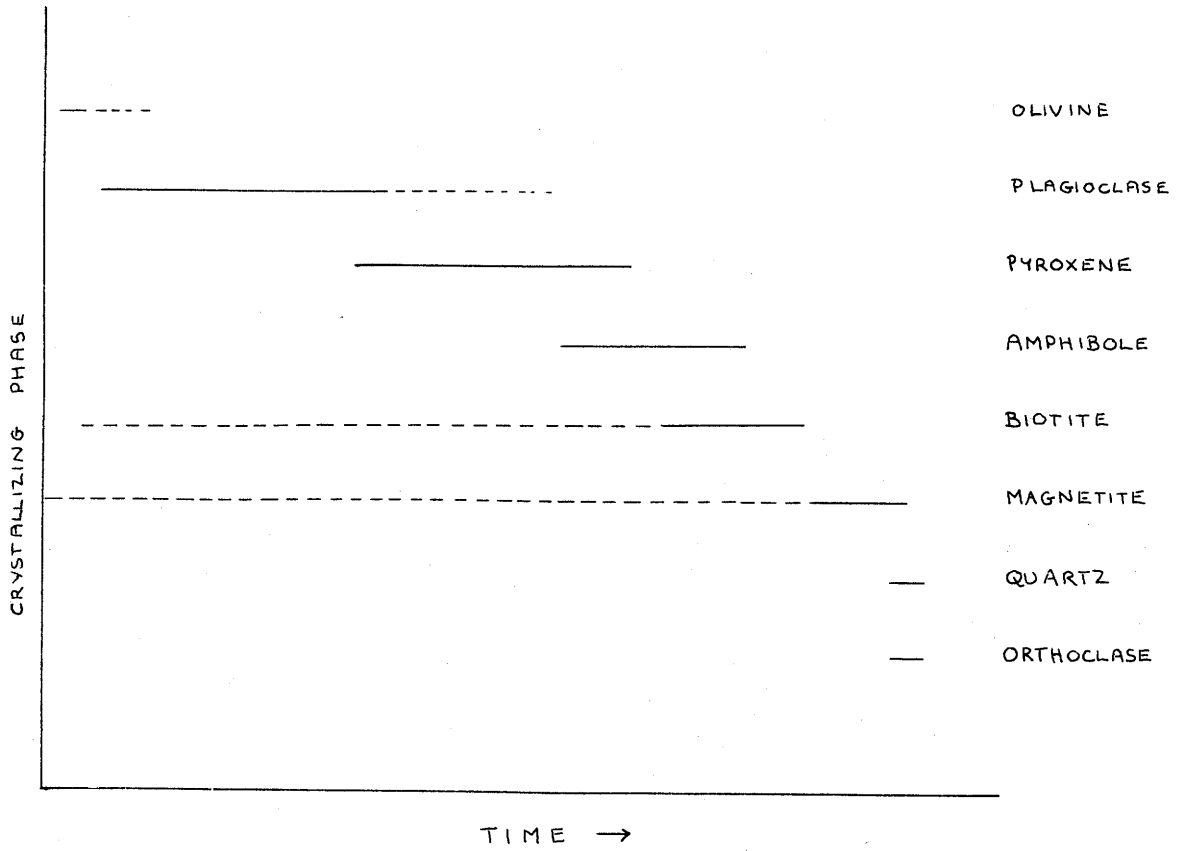
Figure 23. Paragenetic sequence in layered gabbro, as inferred from textural relationships. Solid lines represent major crystallization; broken lines minor crystallization.

It does not seem that any of the above theories can be applied to the layered gabbro at Cape Neddick. Any theory of its formation must explain the following:

(i)   Vertical layering

(ii)   Very small scale of layering

(iii)   Initial oscillatory zoning, followed by irregular crystallization, in the plagioclase

(iv)   Alternate concentrations of plagioclase and ferromagnesian minerals

(v)   Slight iron enrichment of pyroxene in dark layers

(vi)   Greater content of hornblende in dark layers.

The theories outlined above are considered inapplicable for the following reasons:

(i)   Gravity settling would not produce vertical layers.

(ii)   Even if the layers were originally horizontal, and have subsequently been deformed as suggested by Hussey (1961), gravity settling would be apparent as graded layering. Graded layering, although present in the complex, is much rarer than non-graded. Also, gravity settling would result in parallelism of tabular crystals with the layering plane. This has not been detected in the present study, although universal-stage work on optic plane orientation would be necessary to confirm its absence.

(iii)   Gravity settling of plagioclase is a slow process (estimated at 92m/year by Wager and Brown (1968)) and it is hard to see how a slow settling process, combined with a long-period mechanism such as convection currents or periodic volcanic activity, could produce the very small scale layers at Cape Neddick. The scale of layering to which such theories have been applied is of the order of feet rather than inches.

(iv)   Periodic release, or influx, of magma would produce a sudden change in conditions so that layers should be sharply bounded. Those at Cape Neddick are comparatively ill defined.

As an alternative to these theories, the following simplified
model is prepared, and is illustrated in Figure 24.

Magma of composition corresponding to 18% diopside (Di),
24.5% albite (Ab) and 57.5% anorthite (An) was injected into
the Kittery metasediments. This composition was computed from
a spectrochemical analysis of a portion of the normal gabbro,
given by Woodard (1968) in connection with his investigation
of contact reactions. The CIPW norm was obtained using a
computer program written by Luth and Diness and revised by
C. M. Spooner (personal communication), and was recalculated
to 100%(Di + Ab + An).

As this liquid cooled, plagioclase of composition ~ An_{75}
(most calcic composition of plagioclase cores) crystallized first.
If conditions of steady fractionation were maintained, plagio-
clase of increasingly sodic composition would continue to
crystallize until the three-phase boundary in the system
Di-Ab-An (see Figure 24a) was reached. At this point cotectic
crystallization of pyroxene and plagioclase would take place
along the boundary until all the liquid was used up. However,
the extremely irregular nature of the plagioclase crystals
indicates that conditions of crystallization were more com-
plex.

Oscillatory zoning in plagioclase feldspar has been dis-
cussed by Phemister (1934), and a possible explanation is
compound stages of precipitation, each involving two thin
shells of more and less calcic compositions. This results
from a lack of balance between rate of diffusion of ions and
rate of crystallization. A process such as this is envisaged
to account for the oscillatory zoning observed in the Cape
Neddick feldspar, and occurred during the early stages of
crystallization. As magma continued to be injected, the
growing crystals were subjected to turbulent motion, continually
being brought into contact with fresh magma more calcic than
the crystal rims, which were thus resorbed. As the magma
became more sodic recrystallization occurred, resulting in
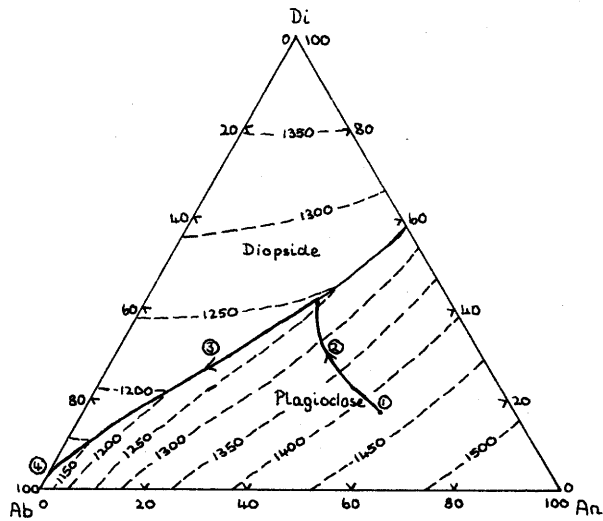the observed irregularity.

Figure 24.a. System diopside-albite-anorthite, showing hypothetical stages in fractional crystallization of gabbro.
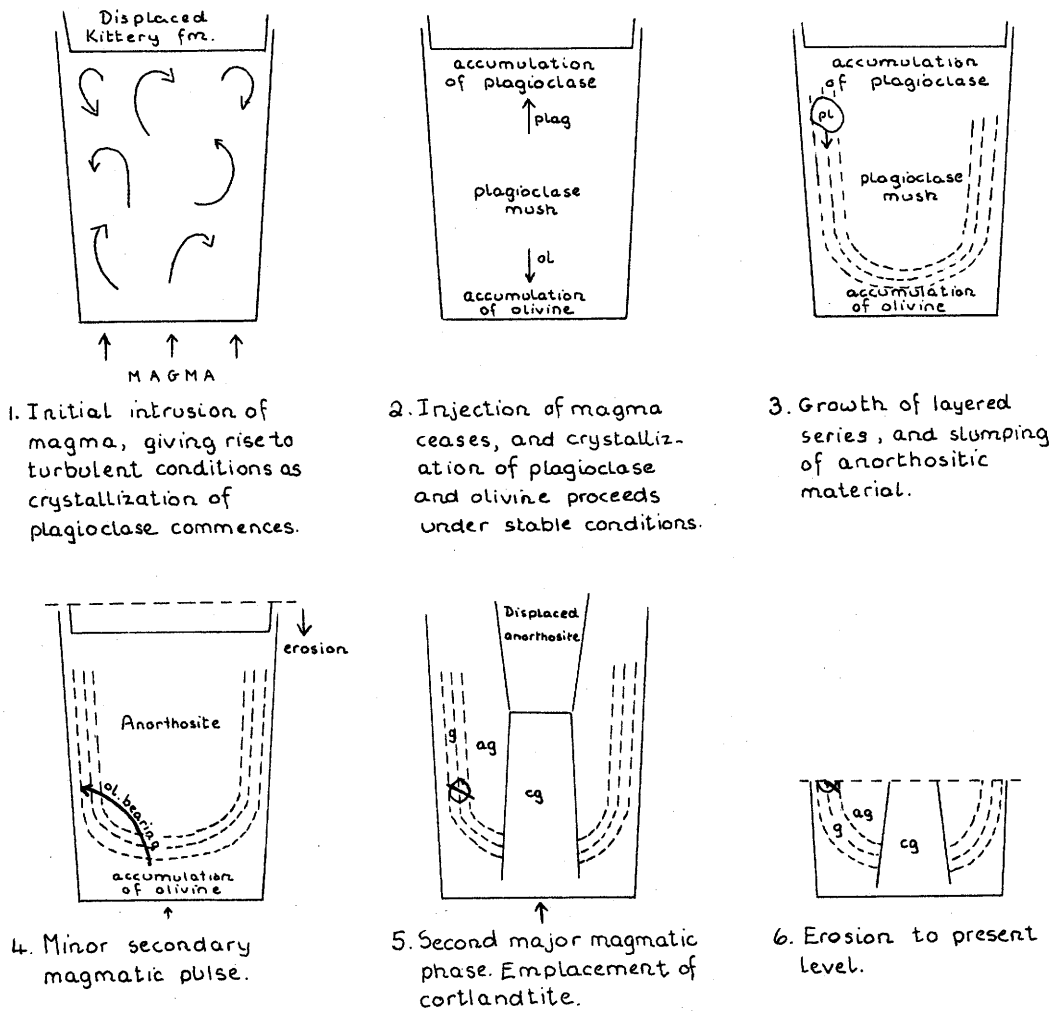

1. Initial intrusion of magma, giving rise to turbulent conditions as crystallization of plagioclase commences.

2. Injection of magma ceases, and crystallization of plagioclase and olivine proceeds under stable conditions.

3. Growth of layered series, and slumping of anorthositic material.

4. Minor secondary magmatic pulse.

5. Second major magmatic phase. Emplacement of cortlandtite.

6. Erosion to present level.

Figure 24.b. Hypothetical mechanism for emplacement and differentiation of gabbro.

After the turbulent injection period, crystallization proceeded under stable conditions. The plagioclase crystals continued to grow as an orthocumulate (defined by Wager (1963), and meaning growth by addition of successively more sodic rims). It is postulated that the plagioclase grains were lighter than the more mafic liquid and thus tended to rise toward the roof of the chamber. A little olivine also crystallized out early. Peck, Wright and Moore (1966), in studying crystallization of basalt in Aloe lava lake, Hawaii, have found evidence of crystal setting of olivine microphenocrysts in the lower part of the lake. It is therefore suggested that the olivine in the Cape Neddick magma chamber likewise tended to sink.

This static crystallization proceeded inwards from the contacts of the intrusion as follows: Consider successive layers in the liquid (1, 2, 3 etc) at increasing distance from the contact. The liquid is already a "mush" of randomly oriented plagioclase grains. Layer 1 reaches the eutectic temperature first and pyroxene crystallizes out together with plagioclase, in the interstices of the plagioclase matrix. Mg^{2+} ions diffuse in from layer 2 to form the pyroxene crystals, leaving layer 2 slightly deficient in Mg^{2+}, but enriched in Fe^{2+} and H_2O. The rate of diffusion of ions from 1 to 2 is greater than the rate of fall of temperature of 2. Thus when 2 reaches the eutectic temperature, the crystals formed will be enriched in Fe^{2+}, and will grow under a slightly higher water pressure (P_{H_2O}). Experiments by Yoder and Tilley (1962) have shown that increase in water content tends to inhibit crystallization of plagioclase, and favors formation of amphibole in place of, or associated with, pyroxene. In a run using the 1921 lava of Kilauea volcano, Hawaii, held at 1000°C and 5000 bars P_{H_2O} for 18 hours, they obtained clinopyroxene rimmed by amphibole, in a manner very similar to that observed in the Cape Neddick sections.

Thus layer 2 consists of a smaller proportion of plagioclase, a greater proportion of hornblende, and iron-enriched

pyroxene, as compared to 1. As 2 forms, Fe^{2+} and H_2O ions diffuse into it from 3. The rate of diffusion is greater than the rate of fall of temperature of 3 so that this becomes depleted in Fe^{2+} and H_2O. When the eutectic temperature is reached in 3 therefore, the pyroxene is magnesium enriched, and little amphibole, but a larger proportion of plagioclase crystallize. In this way successive layers are built up, with regularly fluctuating composition determined by lack of balance between rate of ionic diffusion in the particular layer, and rate of fall of temperature in that layer. Occasionally blocks of anorthositic material, from the initial concentration of plagioclase at the top of the chamber, fall into the crystallizing layered series. This may be a result of decreasing pressure as crystals form, with resulting decrease in density of the liquid phase so that the overlying plagioclase accumulation is mechanically unstable. Such an origin is suggested for the block of light-colored material in area 'A'.

The composition of the crystallizing mass becomes more anorthositic as it moves down the three-phase boundary, so that the center region consists largely of plagioclase (anorthositic unit).

Origin of Anomaly

It is proposed that the anomaly investigated is the result of a second, minor magmatic phase. This caused some of the slightly olivine rich accumulation at the base of the chamber to intrude olivine-deficient material above. Movements like this during the solidification process produce effects of strain, such as shown in the biotite grain in Figure 25, and possibly the brecciated aggregates of plagioclase as shown in Figure 7.
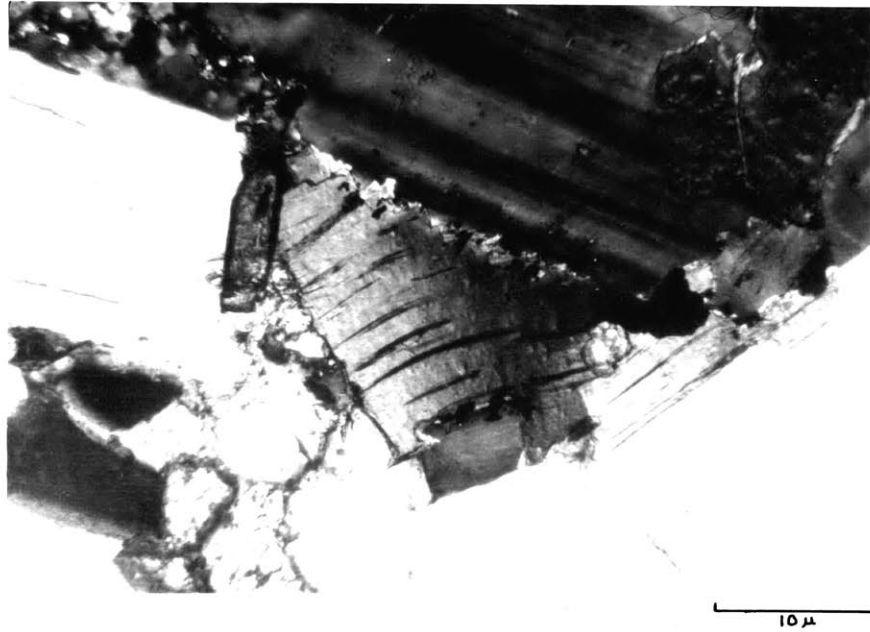
Figure 25. Strained biotite grain. Section 10. Cross nicols. × 138.

Conclusion

It is proposed that differentiation of layers in the
Cape Neddick gabbro is a result of lack of balance between
ionic diffusion and rate of fall of temperature. Both graded
and non-graded layering could be determined by this process,
the graded layering being a result of a fluctuating, rather
than steady, gradient. Anomalies which resemble cross bed-
ding are caused by motion of the crystallizing magma;
anomalies such as the one investigated result from re-intrusion
of magma. Light colored areas in the normal gabbro may rep-
resent slump blocks of overlying anorthositic material. The
anorthositic unit of the complex is an in situ differentiate
of the normal gabbro; the cortlandtitic unit is the result
of a later intrusion of olivine-rich magma.

X-ray analyses of hornblende and biotite might indicate
significant variations in their composition, and study of
detailed mineralogy over a much larger area of the complex
is needed to indicate whether variations are consistent.
The problem of the needle-like inclusions in pyroxene re-
mains unsolved, and single-crystal x-ray techniques might
prove useful here. The relationship of the cortlandtitic
magma to the normal-anorthositic magma (are they two separate
magmas, or differentiates of the same magma?) is an important
question which study of trace element distribution (presently
being carried out by F. A. Frey and R. Zielinski at M.I.T.)
may help resolve.

Acknowledgements

References

Bowen, N. L., 1915: The crystallization of haplobasaltic, haplodioritic and related magmas. Am. J. Sci. (4th ser.), 40, 161-185.

Brown, G. M., 1956: The layered ultrabasic rocks of Rhum, Inner Hebrides. Roy. Soc. Lond. Phil. Trans., Ser. B, 240, 1-53.

Brown, G. M., 1960: The effect of ion substitution on the unit cell dimensions of the common clinopyroxenes. Am. Min., 45, 15-38.

Chayes, Felix, 1956: Petrographic modal analyses. John Wiley and Sons Inc., New York, 113p.

Deer, W. A., R. A. Howie and J. Zussmann, 1963: Rock-forming minerals. Vol. 2. Chain silicates. Green and Co. Ltd., London, 379p.

Deer, W. A., R. A. Howie and J. Zussmann, 1963: Rock-forming minerals. Vol. 4. Framework silicates. Green and Co. Ltd., London, 435p.

Duparc, L., and M. Reinhard, 1924: La détermination des plagioclases dans les coupes minces. Mém. Soc. de Physique et d'Historie Naturelle de Génève, 40, Fasc. 1, 149p.

Eldridge, William F., 1960: A petrographic study of the Cape Neddick gabbro pluton. Unpublished B. A. thesis, University of New Hampshire.

Evans, H. T., Jr., D. E. Appelman and D. S. Handwerker, 1963: The least squares refinement of crystal unit cells with powder diffraction data by an automatic computer index-ing method. (Abstr.). Amer. Cryst. Assoc., Cambridge, Mass., Ann. Meet., Program, p. 42-43.

Gaudette, Henri E., and Carleton C. Chapman, 1964: Web joint pattern of the Cape Neddick gabbro complex, southwestern Maine. Trans. Illinois State Acad. Sci., 57, no. 4, 203-207.

Gaudette, Henri E., and Herbert C. Sakrison, 1959: A structural study of the Cape Neddick gabbro stock. Unpublished B. A. thesis, University of New Hampshire.

Haff, John C., 1939: Multiple dikes of Cape Neddick. Bull. Geol. Soc. Am., 50, 465-514.

Haff, John C., 1941: Contaminated complex dike at Cape Neddick, Maine. J. Geol., 8, 835-853.

Haff, John C., 1943: Alkaline vitrophyre dike, Cape Neddick, Maine. Am. Min., 28, 426-436.

Hall, A. Jean, 1941a: The relation between colour and chemical composition in the biotites. Am. Min., 26, 34-41.

Hall, A. Jean, 1941b: The relation between chemical composition and refractive index in the biotites. Am. Min., 26, 34-41.

Hess, H. H., 1960: Stillwater igneous complex, Montana; a quantitative mineralogical study. Geol. Soc. Am. Memoir 80, 230p.

Hussey, Arthur M. II, 1961: Petrology and structure of three basic igneous complexes, southwestern Maine. Unpublished Ph.D. thesis, University of Illinois, 119p.

Hussey, Arthur M. II, 1962: The geology of southern York County, Maine. Maine Geol. Survey, Spec. Geol. Studies Series., no. 4, 67p.

Jackson, Everett D., 1961: Primary textures and mineral associations in the ultramafic zone of the Stillwater complex, Montana. U. S. Geol. Survey Prof. Paper 358, 106p.

Lombaard, B. V., 1934: On the differentiation and relationships of the rocks of the Bushveld igneous complex. Geol. Soc. S. Africa Trans., 37, 5-52.

Moore, Alan, 1968: Rutile exsolution in orthopyroxene. Contrib. Mineral. and Petrol., 17, 233-236.

Peck, D. L., T. L. Wright, and J. G. Moore, 1966: Crystallization of tholeiitic basalt in Aloe lava lake, Hawaii. Bull. Volcanologique., 29, 629-656.

Phemister, James, 1934: Zoning in plagioclase feldspar.
     Min. Mag., 23, 541-555.

Posnjak, E., and Tom F. W. Barth, 1934: Notes on some struc-
     tures of the ilmenite type. Zeit. Krist., 88, 271-280.

Richter, D. H., and K. J. Murata, 1966: Petrography of the
     lavas of the 1959-60 eruption of Kilauea volcano, Hawaii.
     U. S. Geol. Survey Prof. Paper 537-D, 12p.

Wager, L. R., 1953: Layered intrusions. (Notes on three
     lectures given to the Danish Geological Society in Nov.
     1952). Medd. om Grønland, 12, 335-349.

Wager, L. R., 1959: Differing powers of crystal nucleation
     as a factor producing diversity in layered igneous in-
     trusions. Geol. Mag., 96, no. 1, 75-80.

Wager, L. R., 1963: The mechanism of adcumulus growth in the
     layered series of the Skaergaard intrusion. From "Sym-
     posium on layered intrusions", Min. Soc. Am. Spec. Paper,
     1, 1-9.

Wager, L. R., and G. M. Brown, 1968: Layered igneous rocks.
     Oliver and Boyd, Edinburgh and London, 588p.

Wandke, Alfred, 1922a: Intrusive rocks of the Portsmouth
     Basin, Maine and New Hampshire. Am. J. Sci. (5th ser.),
     4, 139-158.

Wandke, Alfred, 1922b: A petrological study of the Cape
     Neddick gabbro. Am. J. Sci. (5th ser.), 4, 295-304.

Wones, D. R., 1963: Physical properties of synthetic biotites
     on the join phlogopite-annite. Am. Min., 48, 1300-1321.

Woodard, H. H., 1968: Contact alteration in the north wall
     of the Cape Neddick gabbro, Maine. J. Geol., 76, 191-
     204.

Yoder, H. S., Jr., and C. E. Tilley, 1962: Origin of basalt
     magmas: An experimental study of natural and synthetic
     rock systems. J. Petrol., 3, 342-532.